

Experimental and numerical studies on shear behaviour of macro-synthetic fibre reinforced prestressed concrete beams

Lakavath, Chandrashekar; Suriya Prakash, S.; Dirar, Samir

DOI:

[10.1016/j.conbuildmat.2021.123313](https://doi.org/10.1016/j.conbuildmat.2021.123313)

License:

Creative Commons: Attribution-NonCommercial-NoDerivs (CC BY-NC-ND)

Document Version

Peer reviewed version

Citation for published version (Harvard):

Lakavath, C, Suriya Prakash, S & Dirar, S 2021, 'Experimental and numerical studies on shear behaviour of macro-synthetic fibre reinforced prestressed concrete beams', *Construction and Building Materials*, vol. 291, 123313. <https://doi.org/10.1016/j.conbuildmat.2021.123313>

[Link to publication on Research at Birmingham portal](#)

General rights

Unless a licence is specified above, all rights (including copyright and moral rights) in this document are retained by the authors and/or the copyright holders. The express permission of the copyright holder must be obtained for any use of this material other than for purposes permitted by law.

- Users may freely distribute the URL that is used to identify this publication.
- Users may download and/or print one copy of the publication from the University of Birmingham research portal for the purpose of private study or non-commercial research.
- User may use extracts from the document in line with the concept of 'fair dealing' under the Copyright, Designs and Patents Act 1988 (?)
- Users may not further distribute the material nor use it for the purposes of commercial gain.

Where a licence is displayed above, please note the terms and conditions of the licence govern your use of this document.

When citing, please reference the published version.

Take down policy

While the University of Birmingham exercises care and attention in making items available there are rare occasions when an item has been uploaded in error or has been deemed to be commercially or otherwise sensitive.

If you believe that this is the case for this document, please contact UBIRA@lists.bham.ac.uk providing details and we will remove access to the work immediately and investigate.

EXPERIMENTAL AND NUMERICAL STUDIES ON SHEAR BEHAVIOUR OF MACRO-SYNTHETIC FIBRE REINFORCED PRESTRESSED CONCRETE BEAMS

Chandrashekhar Lakavath¹, S Suriya Prakash² and Samir Dirar³

¹Research Scholar, Email: ce19resch11007@iith.ac.in

²Professor and Corresponding Author, Email: suriyap@ce.iith.ac.in

³Associate Professor, Email: s.m.o.h.dirar@bham.ac.uk

^{1,2}Civil Engineering Department, Indian Institute of Technology Hyderabad, India, 502 285.

³Civil Engineering Department, University of Birmingham, Birmingham B15 2TT, UK.

ABSTRACT

Experimental and numerical studies on shear behaviour of macro synthetic fibre reinforced prestressed concrete (MSFRPC) beams are presented. MSFRPC beams are tested at a shear span to depth ratio (a/d) of 2.4 to understand the role of macro synthetic polyolefin fibres on the shear resistance and failure modes. The fibre volume fraction of 0.0%, 0.5%, 1.0% and 1.5% are considered as study parameters. A three-dimensional nonlinear finite element (FE) analysis is carried out to understand the influence of fibres on shear behaviour using the concrete damage plasticity model. Tensile constitutive relations of FRC is derived using inverse analysis from fracture test results and used as input in the FE model. A stage-wise analysis is conducted to include the effects of prestressing and applied external shear loads. The results from FE analysis showed a good agreement with experimental results for different fibre dosages. The effect of level of prestressing and varying compressive strength is studied through calibrated FE models. Due to the addition of macro synthetic fibres, no significant improvement in compressive strength is observed. Low fibre volume addition of 0.5% did not produce an appreciable improvement in shear behaviour. However, test and FE results of beams with higher volume fractions of 1.0% and 1.5% significantly improved the post-cracking behaviour, ductility, and ultimate shear resistance of MSFRPC beams.

Keywords: ABAQUS, Concrete damage plasticity, DIC, Shear, Prestressed concrete beams, Polyolefin fibres.

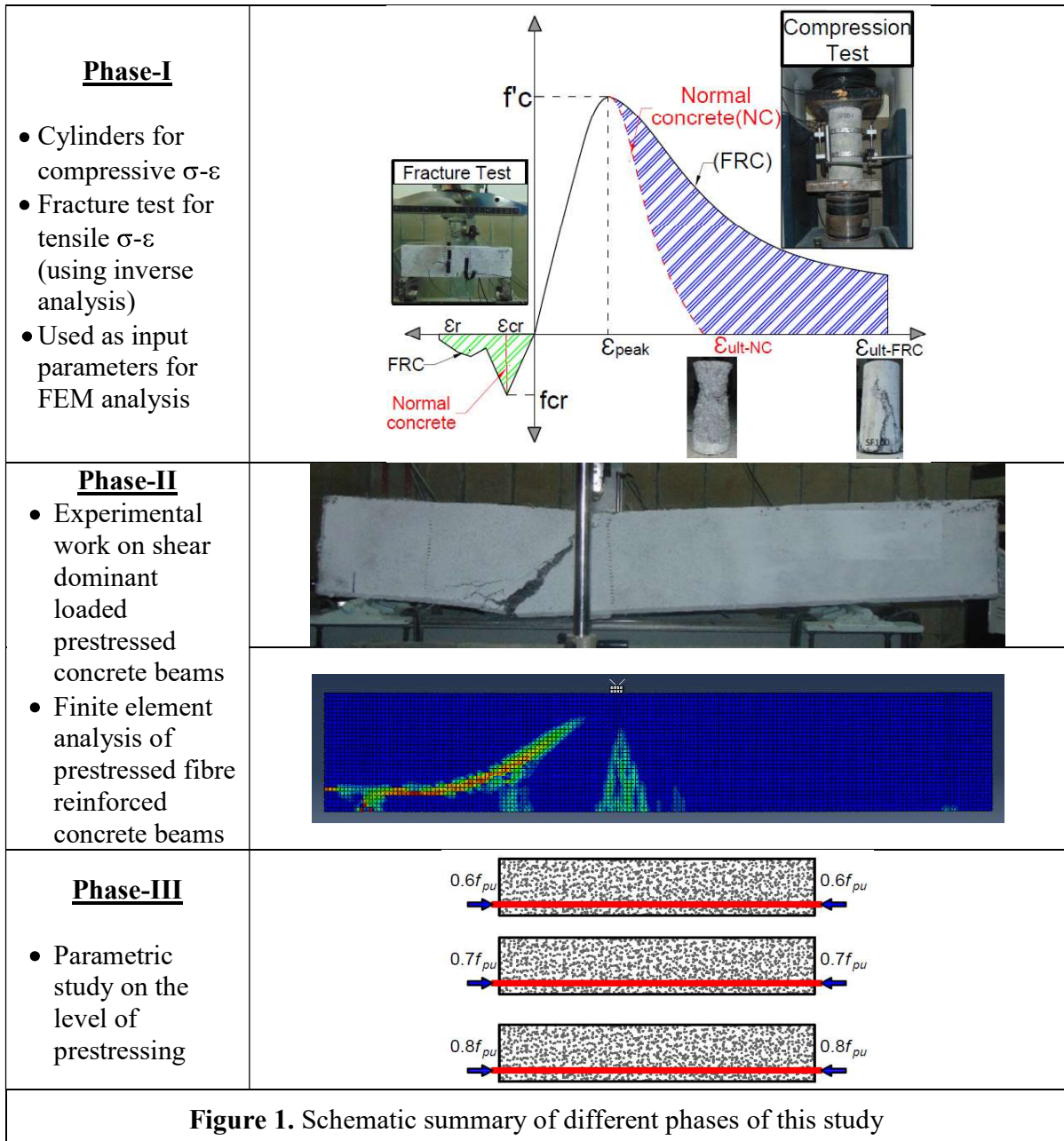
1
2
3
4
5
6
7
8
9
10
11
12
13
14
15
16
17
18
19
20
21
22
23
24
25
26
27
28
29
30
31
32
33
34
35
36
37
38
39
40
41
42
43
44
45
46
47
48
49
50
51
52
53
54
55
56
57
58
59
60
61
62
63
64
65

31 **1.0 INTRODUCTION**

32 High-strength prestressed concrete (PC) beams are commonly used in various prestressing
33 applications [1–3]. Though the use of high-strength concrete has several advantages, it increases
34 the brittle behaviour of PC members. PC beams can fail in a brittle manner under shear dominant
35 loading [1,2,4–6]. The shear behaviour and failure modes of the PC beam depends on various
36 parameters such as compressive strength of concrete, longitudinal and shear reinforcement ratio,
37 level of prestressing, and level of flexure to the shear stress ratio at the critical section. This study
38 tries to understand the shear behaviour of macro-synthetic fibre reinforced prestressed concrete
39 (MSFRPC) beams. Adding discrete fibres in concrete can ensure adequate ductility of prestressed
40 concrete members under various loading conditions.

41
42 The use of fibre-reinforced concrete (FRC) in prestressing application can improve the ductile
43 performance by preventing crack progression. Previous studies on FRC highlighted the beneficial
44 effects of fibres on improving the performance of concrete at both the material and member level
45 [7–15]. ACI provisions [16] suggest a minimum of 0.75% of the volume fraction of steel fibres
46 for replacing the stirrups [15,17]. Lakavath et al. [18] previously investigated the influence of steel
47 and hybrid fibres on the shear behaviour of prestressed concrete beams. A significant improvement
48 in shear capacity was observed due to the addition of 0.5% and 1.0% volume fraction of steel
49 fibres. While the remarkable mechanical performance of steel fibre addition to concrete is
50 recognized, such a combination has durability issues. Steel is not only highly corrodible but also
51 costly to purchase, store and handle. Durability issues associated with SFRC have forced the
52 manufacturers and engineers to develop a variety of fibres with specific properties for
53 construction-related applications. Synthetic fibres such as polyolefin-based macro-synthetic fibre

54 types can solve the issues of reduced workability of FRC and corrosion without significantly
 55 compromising the structural performance. Studies in the past [19–25] have showcased that
 56 synthetic fibre reinforced concrete (SynFRC) is cost-effective in improving the tensile behaviour
 57 of concrete.



58

1
2
3
4 59 Only a few authors in the past have focused on modifications of plasticity-based constitutive
5
6 60 models [26]. The existing continuum plasticity damage model [27,28], such as the concrete
7
8
9 61 damage plasticity (CDP) model, is used in this study. Only a few researchers in the past have used
10
11 62 calibrated tensile constitutive behaviour of FRC in FEM simulations through inverse analysis [29].
12
13
14 63 The schematic presentation of different phases involved in this study is shown in **Figure 1**. Phase-
15
16 64 I includes the material characterization of FRC in compression and tension. Phase-II consists of
17
18
19 65 experimental studies on prestressed concrete beams with different fibre dosages at shear span to
20
21 66 depth ratio of 2.4 and validation with finite element analysis. Finally, Phase-III includes parametric
22
23
24 67 studies.
25
26 68

29 69 **2.0 RESEARCH SIGNIFICANCE**

30
31 70 Only minimal information exists on the behaviour of macro synthetic fibre-reinforced prestressed
32
33
34 71 concrete beams subjected to shear dominant loads. Thus, macro-synthetic fibres reinforced
35
36 72 prestressed concrete beams are tested under shear dominant loading ($a/d=2.4$ to fill the existing
37
38
39 73 knowledge gap. Besides, fracture tests are conducted as well to understand the role of fibres in
40
41 74 crack arresting. The main parameter considered in this study are different volume fraction of fibres
42
43 75 such as ($V_f = 0.0\%$, 0.5% , 1.0% and 1.5%). However, all other parameters such as compressive
44
45
46 76 strength, dimensions of beam, and shear span to depth ratio are kept constant. The key observations
47
48 77 due to the addition of fibres include variations in ductility, toughness, failure mode, and capacity
49
50
51 78 of beams. Hence, the specific objectives of the present study are:

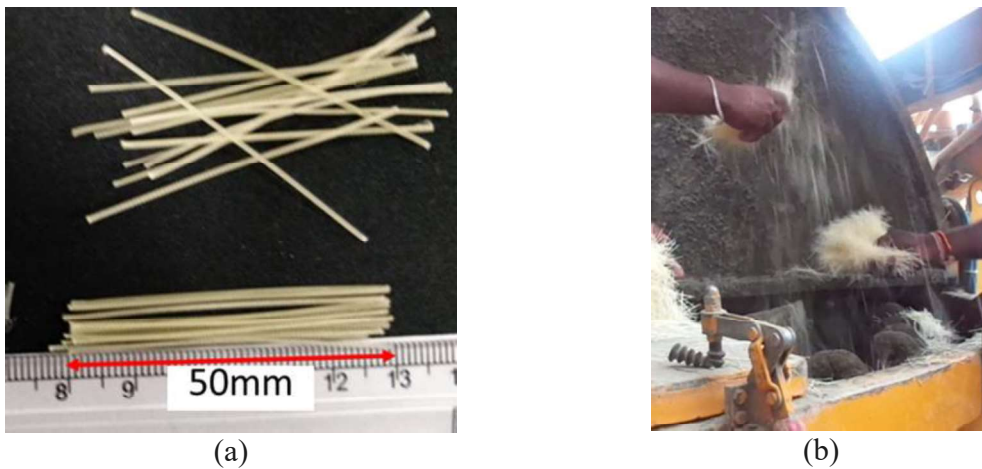
- 52
53 79 1. To understand the effectiveness of macro-synthetic fibres in improving the shear behaviour
54
55 80 of prestressed concrete beams by carrying out experimental studies.

- 1
2
3
4 81 2. To monitor the crack initiation and its propagation in notched prism beams and full-scale
5
6
7 82 prestressed concrete beams using digital image correlation technique (DIC).
8
9 83 3. To utilize the multi-linear stress-strain model (based on fracture tests) as an input for the
10
11 84 nonlinear finite element analysis to simulate the shear behaviour of MSFRPC beams.
12
13
14 85 4. To carry out parametric studies on the influence of level of prestressing force on the shear
15
16 86 behaviour of MSFRPC beams.
17
18
19 87

21 88 **3.0 EXPERIMENTAL PROGRAM**

23 89 Pretensioned beams of dimensions 150 mm x 300 mm x 1600 mm were cast in the precast factory
24
25
26 90 and tested in heavy structures lab at the Indian Institute of Technology Hyderabad. Eight beams
27
28 91 were tested at a shear span to depth (a/d) ratio of 2.4. As per Kani's classical theory [30], the a/d
29
30 92 ratio of 2.5 is the transition point below which the RC beams fail in a shear critical mode.
31
32
33 93 Therefore, a/d ratio of 2.4 is considered in this study to avoid arch action and ensure diagonal shear
34
35 94 tension (DST) mode [31,32]. The variables considered in this study are 0.0%, 0.5%, 1.0% and
36
37
38 95 1.5% of volume fraction (V_f) of macro-synthetic fibres (MSF). In this study, MSF100 represents
39
40 96 prestressed concrete beams reinforced with macro synthetic fibres of 1.0% by concrete volume.
41
42
43 97 The concrete mix was designed to attain a strength of 50 MPa as per the Indian standard IS 10262
44
45 98 [33]. The design concrete mix includes the fine aggregates, coarse aggregate, cement,
46
47 99 superplasticizer, and water content as detailed in **Table 1**. All the materials were added in the
48
49
50 100 following sequence to avoid the balling effect. Firstly, the total quantity of coarse aggregates, fine
51
52 101 aggregates, and cement was added, followed by 50% of the total water quantity. Afterwards, macro
53
54 102 synthetic fibres were added manually, as shown in **Figure 2(b)**. Finally, the remaining water and
55
56 103 superplasticizers were added to the pan mixture. Details of fibre and manual addition of fibres to
57
58
59
60
61
62
63
64
65

1
2
3
4 104 the concrete while mixing is shown in **Figure 2**. The obtained target cube compressive strength is
5
6
7 105 58 MPa. In the same mix, the fibre volume of 0.5% (4.55 kg/m³), 1.0% (9.1 kg/m³) and 1.5%
8
9 106 (13.65 kg/m³) were added. The compressive strength of concrete cubes are 59 MPa, 67 MPa and
10
11
12 107 68 MPa, respectively. The properties of the macro-synthetic fibres in this study are shown in **Table**
13
14 108 **2**.



17
18
19
20
21
22
23
24
25
26
27
28
29
30
31
32
33
34
35
36 110
37 111 **Figure 2.** Macro synthetic fibers (MSF) (a) Geometry (b) Mixing of MSF to concrete

38
39
40
41
42
43
44
45 112 **Table 1.** Concrete mix proportion in kg/m³

Cement	CSS	NRS	Coarse aggregate		SP	Water	Macro-synthetic fibre (MSF) ($V_f = 0\%, 0.5\%, 1.0\%$ and 1.5%)
			20 mm	10 mm			
450	415	312	755	355	2.6	152	0.0, 4.55, 9.1 and 13.65

46
47
48 113 Note: CSS= Crushed stone sand, NRS= Natural River Sand, SP= Super Plasticizer

49
50
51
52
53
54
55
56
57
58
59
60
61
62
63
64
65 **Table 2.** Properties of macro-synthetic fibre (Polyolefin fibres)

Specification	Macro-synthetic fibre (MSF)
Specific gravity	0.91
Length (mm)	50
Diameter (mm)	0.5
Tensile strength (MPa)	618
Modulus of elasticity (GPa)	10
Aspect ratio	100

1
2
3
4
5
6
7
8
9
10
11
12
13
14
15
16
17
18
19
20
21
22
23
24
25
26
27
28
29
30
31
32
33
34
35
36
37
38
39
40
41
42
43
44
45
46
47
48
49
50
51
52
53
54
55
56
57
58
59
60
61
62
63
64
65

114 **3.1 Compression Tests on Concrete Cylinders**

115 Concrete cylinders of size 150 mm (diameter) x 300 mm (length) were tested under uniaxial
116 compression to understand the effect of macro synthetic fibres in improving the strength and
117 ductility. All the cylinders were tested in displacement control mode with a rate of 1 mm/min,
118 using a servo-controlled compression testing machine of 500 kN capacity. Three linear variable
119 displacement transducers (LVDT) are attached to cylinders for monitoring the axial deformation.
120 Average compressive stress-strain curves are shown in **Figure 3**. Test results revealed that the
121 addition of fibres does not significantly influence the cylinder compressive strength. However, the
122 compressive toughness index increased from 1.4 to 5.7 times due to the addition of macro synthetic
123 fibres (**Table 3**). The toughness of MSF50 increased by 40% when compared to control cylinders
124 due to the addition of 0.5% fibre volume dosage. However, the ultimate strain of MSF50 did not
125 increase as that of MSF100 and MSF150 (**Figure 3**). In MSF50 specimens, the crack bridging and
126 passive confinement offered by fibres was not effective to significantly increase the post-peak
127 behaviour. Hence, the increment in toughness was not significant compared to higher dosages. The
128 failure modes of cylinders due to the addition of fibres are shown in **Figure 3**. The peak
129 compressive strength of the cylinder is in the range of 52 MPa - 54 MPa.

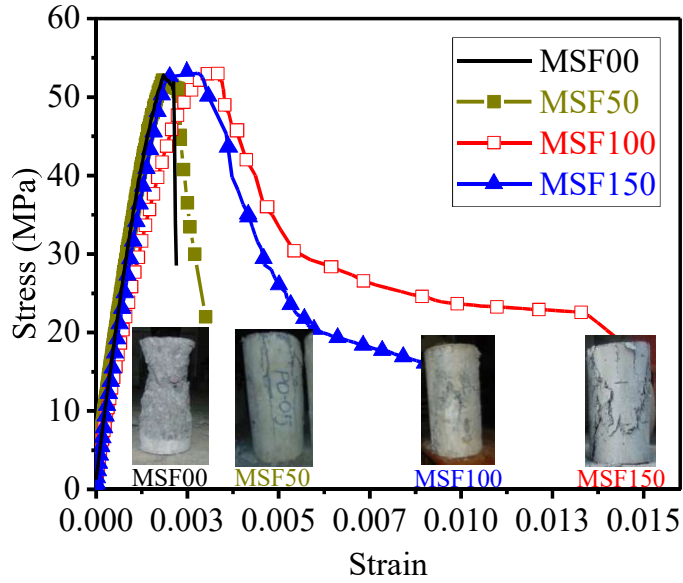


Figure 3. Stress-strain curve of concrete cylinders in compression

Table 3. Properties of MSFRC in Compression

Mix ID	Cube strength (MPa)	SD (MPa)	Cylinder strength (MPa)	SD (MPa)	Toughness (A_f)	Toughness index ($T.I = A_f/A_c$)
MSF00	57.91	1.46	52.75	1.05	0.0738	1.00
MSF50	59.23	1.30	53.46	1.26	0.1028	1.40
MSF100	67.08	1.27	53.62	0.83	0.2805	3.80
MSF150	68.12	1.18	54.14	1.10	0.4239	5.74

Note: SD = Standard deviation (MPa), A_f = area of the stress-strain curve of the fibre-reinforced concrete cylinder, A_c = area of the stress-strain curve of the control cylinder

The tension stiffening response of fibre reinforced concrete depends on the characteristics of fiber such as aspect ratio, length, types, the volume fraction of fibers, as well as matrix properties such as strength and aggregate size. Few researchers [34–39] in the past have studied the influence of fibre orientation factor on the mechanical performance of FRC, such as strength, load-CMOD, and fracture energy. They noted a considerable improvement in post-peak response due to the orientation effect [34,37,40]. The increment in post-peak response leads to an increase in residual flexural tensile strength (f_R). Thus, the ductility of fibre-reinforced prestressed concrete beams can

1
2
3
4 143 be increased in both flexure and shear dominant loading. However, the effect of fibre orientation
5
6
7 144 is not considered in this study and is scope for further work.
8

9 145

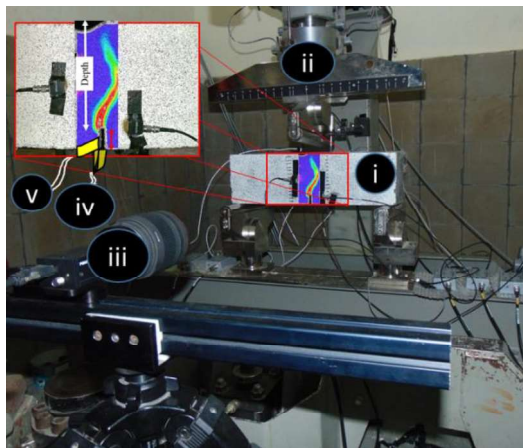
10 11 146 **3.2 Fracture Tests**

12
13
14 147 Concrete prisms were cast and tested under a three-point bending test as per EN14651 (2005). The
15
16 148 size of the prism is 150 mm x 150 mm x 500 mm. A notch of 25 mm depth and 5 mm width was
17
18
19 149 prepared in the prism to localize the damage in a defined position. The crack width is monitored
20
21 150 by crack mouth opening displacement (CMOD) and crack tip opening displacement (CTOD)
22
23
24 151 gauges. Similarly, one LVDT is used to monitor the vertical deflection of the prism. A non-contact
25
26 152 digital image correlation (DIC) technique was used to monitor full-field strain measurements and
27
28
29 153 to study crack propagation. The DIC system consists of two light sources, one high-resolution
30
31 154 camera, and a storage device, as shown in **Figure 4 (a)**. In the pre-processing phase, the notched
32
33
34 155 beams were painted and speckled with black colour ink with a speckling gun [41]. After mounting
35
36 156 all the gauges, the calibration image is captured before the start of testing. After that, images were
37
38
39 157 captured at specific intervals according to the rate of loading. All the FRC prisms were tested under
40
41 158 displacement control mode with a 5mm/min rate by using a flexure testing machine, as shown in
42
43 159 **Figure 4 (a)**.

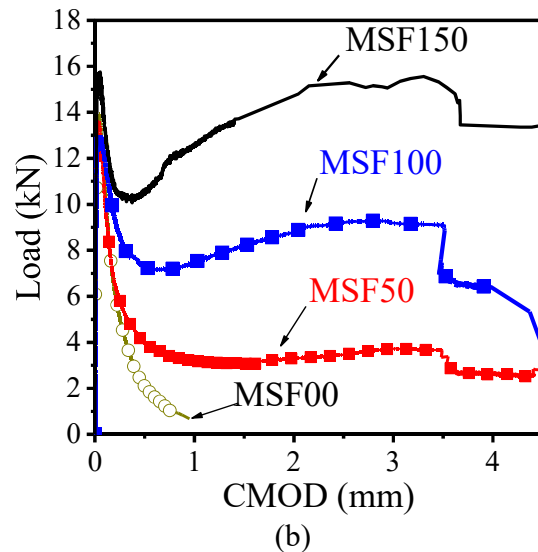
44
45
46 160

47
48 161 The load-CMOD response of MSF00, MSF50, MSF100, and MSF150 concrete prisms are
49
50 162 presented in **Figure 4 (b)**. The response shows that the post cracking behaviour was significantly
51
52
53 163 improved due to the addition of 0.5%, 1.0%, and 1.5% of volume fractions of MSF compared to
54
55
56 164 control (MSF00) beams. In control prisms (MSF00), the obtained peak load is 14 kN, which is the
57
58 165 same as that of the MSF100 prism. However, MSF100 prisms also had a second peak load of 9.31
59
60
61
62
63
64
65

1
2
3
4 166 kN, which occurred at CMOD of 2.3 mm. Thus, macro synthetic fibre addition did not change the
5
6
7 167 first cracking load but significantly improved the post cracking behaviour. Similarly, in MSF50
8
9 168 beams, the second peak load of 4kN is observed at a CMOD of 2.5 mm. Hence, from this
10
11 169 experimental response, it is concluded that the MSF fibres of aspect ratio 100 can effectively
12
13
14 170 engage in strain redistribution at higher crack openings such as 2.5 mm of CMOD. The load-
15
16 171 CMOD curves were used to obtain the tensile stress-strain response from the inverse analysis. The
17
18
19 172 multi-linear tensile stress-strain behaviour of specimens with different fibre volume fractions was
20
21 173 obtained from the inverse analysis. More information on inverse analysis can be found elsewhere
22
23
24 174 [42].
25
26 175



27
28
29
30
31
32
33
34
35
36
37
38
39
40
41
42
43 i. Test Specimen, ii. FTM Actuator, iii. DIC Camera,
44 iv. CTOD Gauge, v. CMOD Gauge



45
46
47
48
49
50
51
52
53
54
55
56
57
58
59
60
61
62
63
64
65
Figure 4. Fracture tests on MSFRC Prisms (a) Test setup, (b) Load-CMOD curve

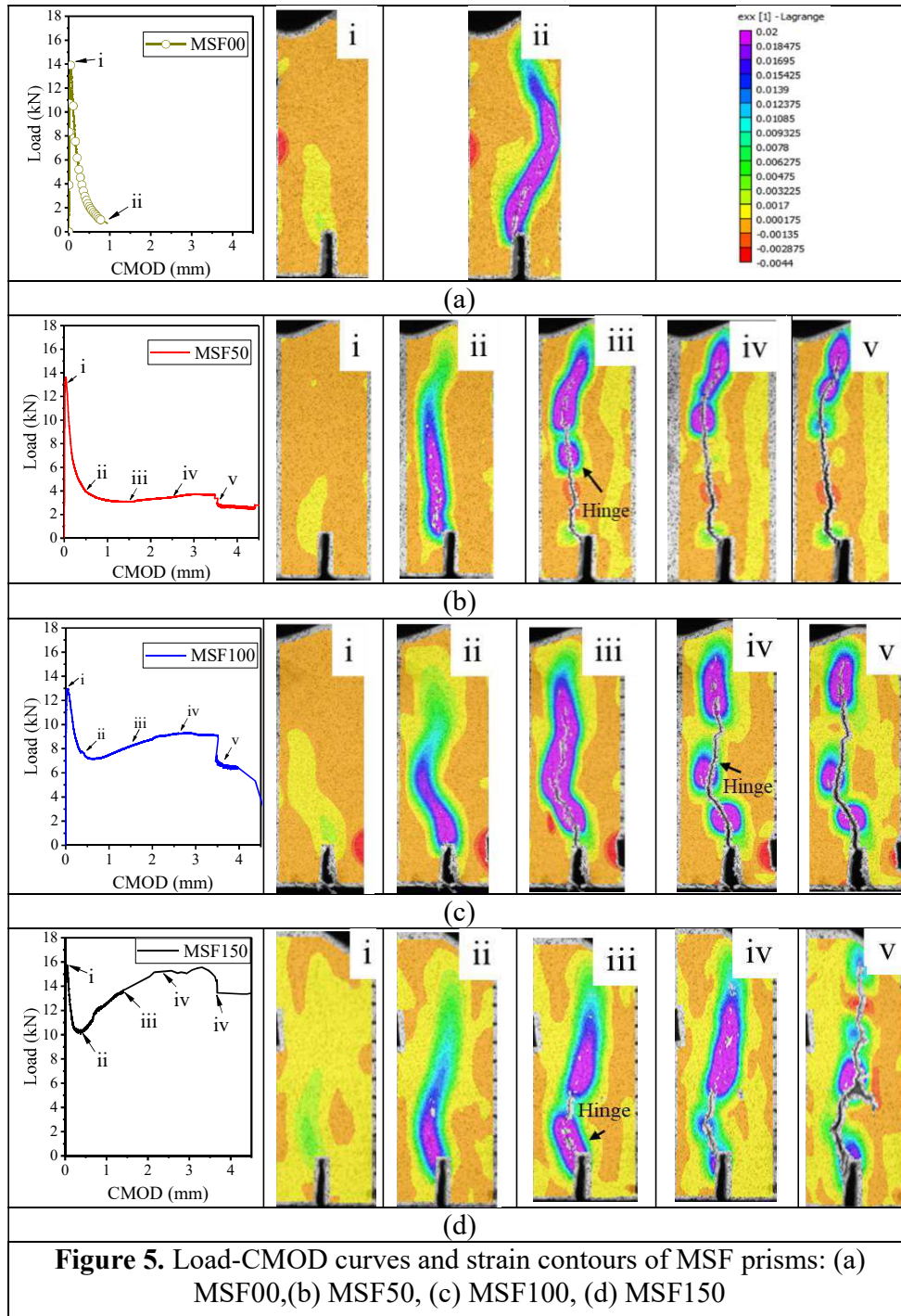
176
177 The average residual flexural tensile strength (f_{R1} to f_{R4}) of MSFRC prisms was calculated based
178 on RILEM recommendation [43]. Here, f_{R1} , f_{R2} , f_{R3} , and f_{R4} are calculated at CMOD of 0.5mm,
179 1.5mm, 2.5mm, and 3.5mm respectively. The fracture energy (G_f) of prisms was calculated based
180 on the provisions of the Japan concrete institute (JCI) code [44]. The improvement in fracture
181 energy due to the addition of 0.5%, 1.0%, and 1.5% volume fraction of MSF fibres are 4.55, 9.62,

1
2
3
4 182 and 16.03 times that of the control prism (MSF00). The residual flexural tensile strength of MSF
5
6
7 183 prism was calculated based on the RILEM [43] recommendations and presented in **Table 4**. The
8
9 184 DIC strain contours were used (**Figure 5**) for understanding the crack initiation and crack
10
11
12 185 propagation at different CMOD values[21].
13
14 186
15
16 187

Table 4. The residual flexural tensile strength and fracture energy of prisms

Mix ID	Residual flexural tensile strength (MPa)				Total fracture energy (N-mm)	The ratio of Fracture Energy (ΔG_f)
	f_{R1}	f_{R2}	f_{R3}	f_{R4}	$G_f (\times 10^{-3})$	$\Delta G_f = \frac{G_f}{G_{fc}}$
MSF00	0.69	-	-	-	156.7	1.00
MSF50	1.14	0.88	1.00	0.97	713.2	4.55
MSF100	2.10	2.36	2.65	2.62	1506.7	9.62
MSF150	3.04	4.00	4.39	4.34	2512.5	16.03

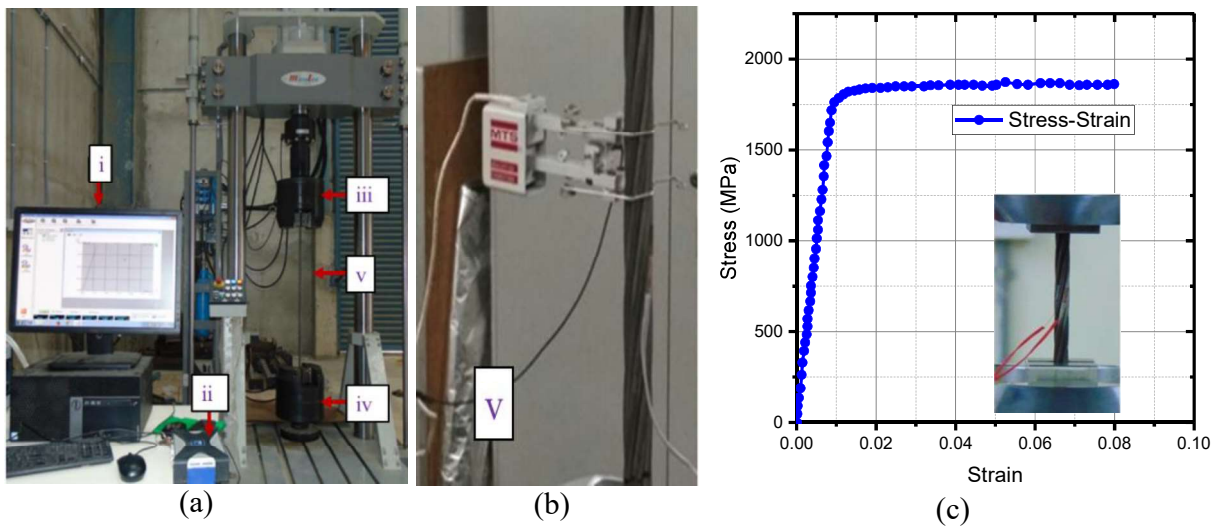
18
19
20
21
22
23
24
25
26
27
28
29
30
31 188
32
33 189 In control prisms (MSF00), the crack propagated without the formation of any strain localization,
34
35
36 190 as shown in **Figure 5 (a)**. However, in the case of MSF50 beams, the strain localization started at
37
38 191 a CMOD of 1.5 mm. Similarly, in MSF100 beams, the number of hinge formations was more
39
40
41 192 along the cracked surface compared to MSF50 beams. The crack initiated and propagated in MSF
42
43 193 beams from the tension zone to the loading point progressively, and the propagation of the tip of
44
45
46 194 the crack can be visualized in **Figure 5**. The strain contours from DIC analysis help understand
47
48 195 the reason for a significant increase in the second peak in loading **Figure 4 (b)-(d)**. The hinges
49
50 196 formed along the depth of the beam due to the bridging action of fibres against the crack opening,
51
52
53 197 as shown in **Figure 5**. The detailed discussion about the formation of hinge and comparison with
54
55 198 different fiber dosages were discussed in the previous work of authors [21].
56
57
58 199



3.3 Stress-Strain Curve of Prestressing Strand

The seven-wire low relaxation prestressing strand of 12.7 mm diameter was tested under tension to get the stress-strain response. An extensometer and strain gauges were mounted to measure the

strains, as shown in **Figure 6 (b)**. The test is performed according to ASTM A1061 [45] with the help of a servo-controlled fatigue testing machine (FTM) as shown in **Figure 6**. The obtained stress-strain response of prestressing strand is shown in **Figure 6 (c)**. The average tensile strength of the prestressing strand is 1860 MP with an elastic modulus of 196 GPa (**Table 5**). The same test results were used for nonlinear finite element analysis simulation after converting the engineering stress-strain curve to the true stress-strain curve.



i-monitor, ii=Data acquisition system, iii=Upperlimb, iv=Lowelimb, v=Prestressing strand with clip-gauge

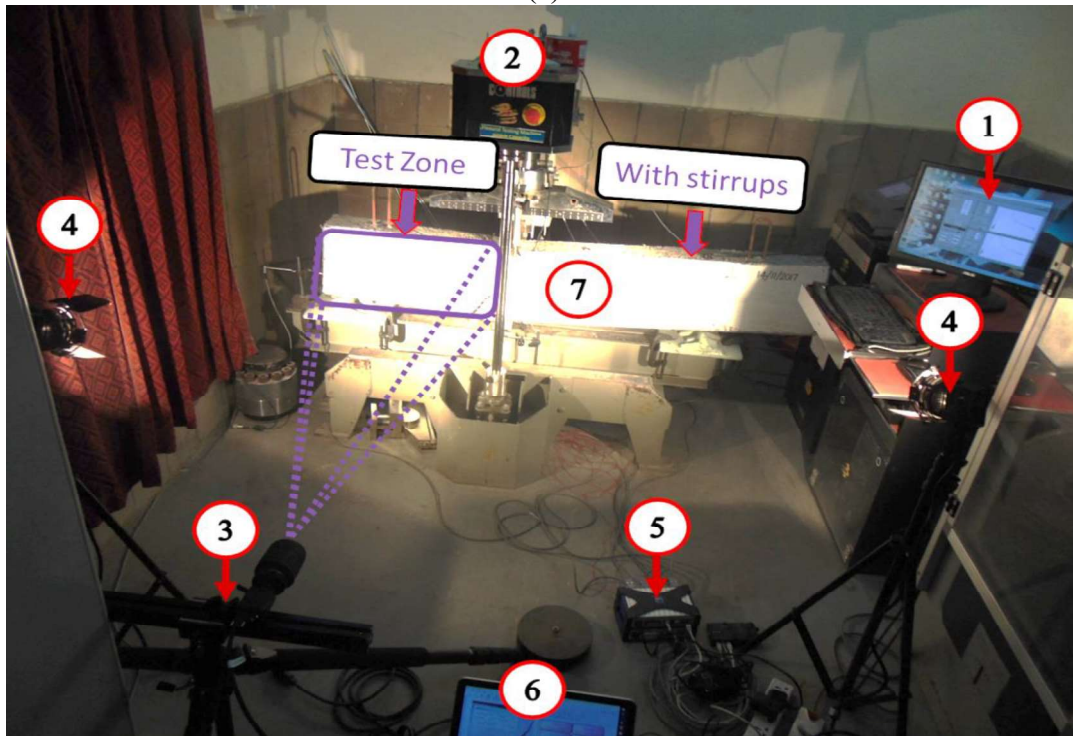
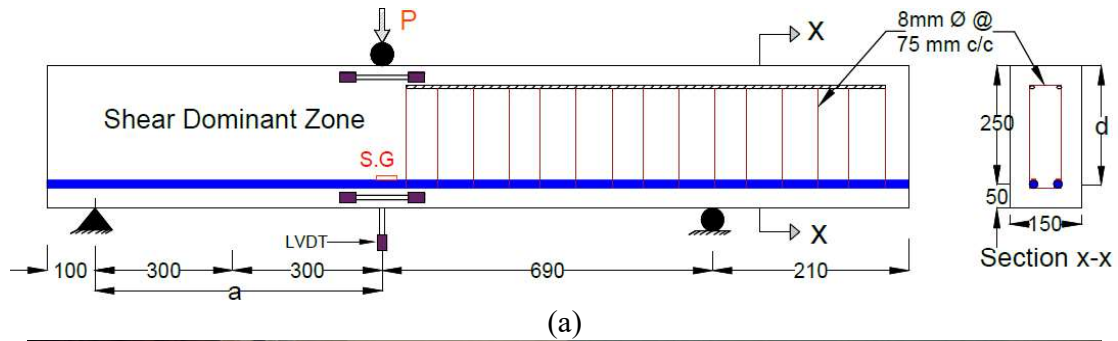
Figure 6. Coupon test of HTS strand: (a) Fatigue testing machine, (b) Extensometer, (c) Prestressing strand stress-strain curve

Table 5. Mechanical properties of prestressing strand

Avg. Tensile strength (MPa)	f_{yp}	1860
Area of cross-section (mm ²)	A_p	98.4
Modulus of elasticity (MPa)	E_p	196500
Poisson's ratio	γ	0.3

1
2
3
4 213 **3.4 Testing of Prestressed Concrete Beams**

5
6 214 The prestressed concrete beams of size 150 mm × 300 mm × 1600 mm were cast with MSFRC
7
8
9 215 concrete (0.0%, 0.5%, 1.0% and 1.5% V_f of macro-synthetic fibers). In total, eight prestressed
10
11 216 concrete beams were tested under shear-dominated loading, as shown in **Figure 7**.
12
13
14 217



52 1. Controller, 2. Test frame of 300KN capacity, 3.DIC camera, 4. The light source, 5. Data Acquisition
53 system (DAC), 6. DAC data storage (DAC+DIC) and 7. Specimen
54
55 (b)

56 **Figure 7.** Prestressed concrete beam details along with (a) Instrumentation, (b) Test setup

57 218

1
2
3
4 219 Two LVDTs were used at the loading point for monitoring the deflection of beams. The strain in
5
6
7 220 strands is monitored using strain gauges bonded on the prestressing strand. The level of
8
9 221 prestressing applied in these beams is 40% to that of the ultimate capacity of the prestressing strand
10
11 222 (1860 MPa). A prestressing force of 154.5 kN was applied at an eccentricity of 100mm. Due to
12
13
14 223 this, average compressive stress of 3.43 MPa is produced. A DIC setup was used for tracking the
15
16 224 crack initiation and propagation and for strain measurements in the test zone. The images of
17
18
19 225 deformed specimens are captured at the same rate of loading in the shear dominant zone of the
20
21 226 specimen. After that, post-processing is carried out by using VIC-2DTM package. All the
22
23
24 227 prestressed concrete beams were tested using displacement control mode at a rate of 0.025mm/sec.
25
26 228 In each series, two prestressed concrete beams were tested to ensure the consistency of test results.
27
28

29 229

30 31 230 **4.0 TEST RESULTS AND DISCUSSION**

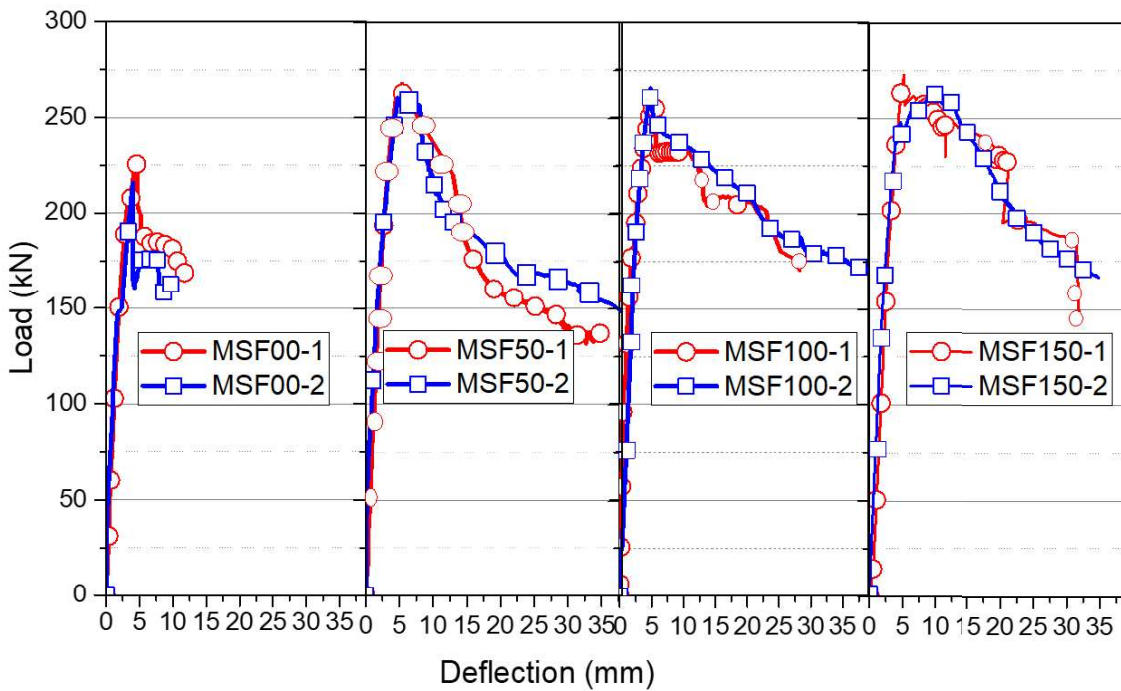
32 33 231 **4.1 Control beam (MSF00)**

34 232 The complete load-deflection response of macro synthetic fibre-reinforced prestressed concrete
35
36 233 (MSFRPC) beams are shown in **Figure 8**. The first shear crack in MSF00 was initiated at a load
37
38
39 234 of 178 kN and deflection of 2.9 mm (**Figure 9**). By strain contours from DIC measurements, the
40
41
42 235 crack initiation and propagation path can be identified. MSF00 reached a peak load of 216.3 kN at
43
44
45 236 a deflection of 4 mm. After reaching the peak load, a shear crack formed at an angle of 41.2° due
46
47
48 237 to diagonal shear tension. The energy absorption capacity is calculated as the area under the load-
49
50
51 238 deflection curve up to the ultimate load point. The ultimate load (P_u) point is considered as a 20%
52
53 239 drop from the peak load (P) [18]. The average energy absorption capacity of the control beam is
54
55 240 measured as 785.8 (kN-mm), and the failure mode is observed as direct shear tension (*DST*).
56
57

58 241

1
2
3
4 242 **4.2 MSFRPC beams (MSF50)**

5
6 243 The load-deformation behaviour of the MS50 beam with a volume fraction of 0.5% is shown in
7
8
9 244 **Figure 8**. The peak load of MSF50 was 264.6 kN at the deflection of 4.8 mm. The peak load
10
11 245 increased by 21.4% when compared with a control beam (MSF00). The first shear crack initiated
12
13
14 246 in MSF50 beams at a load of 160.6 kN at a deflection of 2.1 mm (**Figure 9**). MSF50 reached a
15
16 247 peak load of 264.6 kN at a deflection of 4.8 mm, and shear crack is formed at an angle of 45.8°.
17
18
19 248 The average energy absorption capacity of the MSF50 beam is obtained as 2918.2 kN-mm, which
20
21 249 is 3.72 times more than that of control beams. A low fibre dosage of 0.5% could not change the
22
23
24 250 failure mode, and MSF50 failed in direct shear tension failure mode.

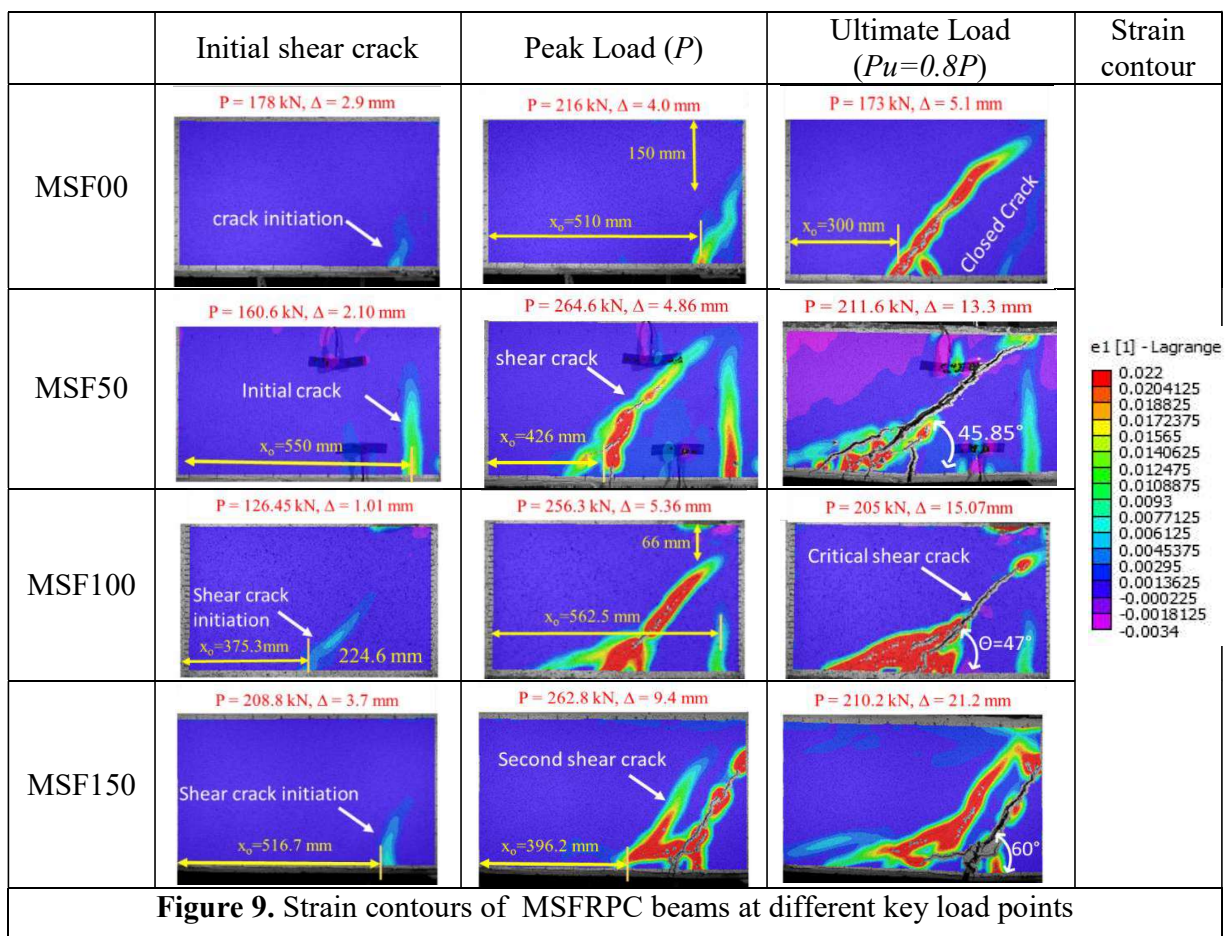


25
26
27
28
29
30
31
32
33
34
35
36
37
38
39
40
41
42
43
44
45
46
47
48
49
50 **Figure 8.** Load-deflection response of PO00, PO50, PO100, and PO150 beams

51 251
52
53 252 **4.3 MSFRPC beams (MSF100)**

54
55
56 253 The shear crack in MSF100 was initiated at a distance of 375.3 mm from the support (**Figure 9**).
57
58 254 The same crack propagated towards the loading point with an angle of 47°. The improvement in
59
60
61
62
63
64
65

255 peak load is 40 kN to that of control beams (216 kN). This increase in peak capacity is due to the
 256 fibre bridging action, which restrained the crack opening. Similarly, the improvement in ultimate
 257 load is about 21.2% to that of the control beam. The strain contour plots of MSF100 beams (**Figure**
 258 **9**) showed more distributed cracks occurred at peak and ultimate load due to the presence of fibres.
 259 Also, the failure angle did not change much even with the addition of high fibre dosage. However,
 260 MSF100 beams failed in the ductile mode, as shown in **Figure 9**.



262 Energy absorption capacity (EAC) also increased significantly due to fibre addition (**Table 6**). The
 263 improvement in EAC due to the addition of 1.0% of macro synthetic fibres is 4.0 times that of
 264 control beams. A significant increase in EAC indicates the addition of fibres helps in absorbing
 265 the sudden energy release (control beams) and thereby converts the brittle failure to ductile mode.

4.4 MSFRPC beams (MSF150)

The MSFRPC beams reinforced with a 1.5% volume fraction of macro synthetic fibres reached a peak load of 272.7 kN. Also, the improvement in EAC is 6.0 times that of control beams. The fibres contributed effectively to strain redistribution, due to which the post-peak response increased reasonably. Similarly, the ultimate load improvement is about 26% to that of the control beam is observed. From the strain distribution plots of MSF150 beams, it is observed that more distributed cracks occurred along with new shear cracks at peak and ultimate load. Moreover, due to the higher dosage of fibre addition, the crack angle of the critical crack increased from 41° to 65°. MS150 beams failed in ductile mode, as shown in **Figure 9**. From experimental results, it is observed that the beam reached its ultimate load at the deflection of 21 mm (**Table 6**).

Table 6. Summary of test results of MSFRPC Beams

Beam ID		A	B	C	D (kN-mm)	θ (°)	Failure mode
MSF00-1	Load (kN)	178	216.3	173.0	785.8	41.2	DST
	Δ (mm)	2.9	4.0	5.1			
MSF00-2	Load (kN)	167	224.5	179.6	741.5	42.4	DST
	Δ (mm)	2.6	4.2	5.3			
MSF50-1	Load (kN)	160.6	262.6	211.6	2918.2	45.8	DST
	Δ (mm)	2.1	4.8	13.3			
MSF50-2	Load (kN)	158.8	260.2	208.2	2298.8	45.0	DST
	Δ (mm)	2.6	4.7	10.9			
MSF100-1	Load (kN)	126.5	256.3	205.0	3183.5	47.5	DST
	Δ (mm)	1.0	5.3	15.0			
MSF100-2	Load (kN)	131.2	262.2	209.7	3184.8	49.3	DST
	Δ (mm)	1.2	5.4	15.2			
MSF150-1	Load (kN)	159.2	272.7	218.2	4742.8	65.3	FS
	Δ (mm)	2.5	5.3	21.4			
MSF150-2	Load (kN)	208.8	262.8	210.2	4733.7	60.2	FS
	Δ (mm)	3.7	9.4	21.2			

Note: A = Shear crack load (kN), B = Peak load (kN), C = Ultimate load (kN), D = Energy absorption capacity (EAC) (kN-mm), θ = Failure crack angle, DST= Direct shear tension, FS=Flexure shear.

1
2
3
4 283 **4.5 Discussion**

5
6
7 284 The control prestressed concrete beams cracked at a distance of 510 mm from support. After peak
8
9 285 load, the new crack is initiated at a distance of 300 mm from support, as shown in **Figure 9**, and
10
11 286 the beam collapsed in brittle mode. However, MSF50 beams with 0.5% volume fraction, a flexural
12
13 287 crack initiated at a distance of 550 mm from support. At peak load point, it cracked in shear at a
14
15 288 distance of 426 mm from support and led to final failure under direct shear tension mode. Similarly,
16
17 289 the MSF100 beams with 1.0% of fibre volume fraction had a shear crack at a distance of 375.3
18
19 290 mm from support but did not fail in a brittle manner. The MSF150 beams had a flexure-shear crack
20
21 291 at a distance of 516.7 mm. With the increase in applied loads, the same crack propagated towards
22
23 292 the loading point at an angle of 60°. Other than MSF100 beams, the critical crack initiation length
24
25 293 increased with an increase in fibre volume fraction. Similarly, the crack propagation rate reduced
26
27 294 with an increase in the dosage of fibres.
28
29
30
31
32

33 295
34
35
36 296 After the failure of specimens, the fibre distribution in a cracked plane is measured to understand
37
38 297 the nature of fibre distribution. The failure plane of prestressed fibre reinforced concrete beams
39
40 298 was divided into several grids, as shown in **Figure 10** with an offset of 50 mm in both horizontal
41
42 299 and vertical directions. The fibre distribution in MSF50 was 65 to 75 numbers in a 50 mm grid.
43
44 300 Similarly, in both MSF100 and MSF150 beams, the number of fibres across the cracked plane
45
46 301 increased significantly, as shown in **Figure 10 (b)**. Fibre distribution was found to be even across
47
48 302 the depth of the failure plane. Both the rupture and pull-out failure of fibres were observed.
49
50
51
52

53 303
54
55
56
57
58
59
60
61
62
63
64
65

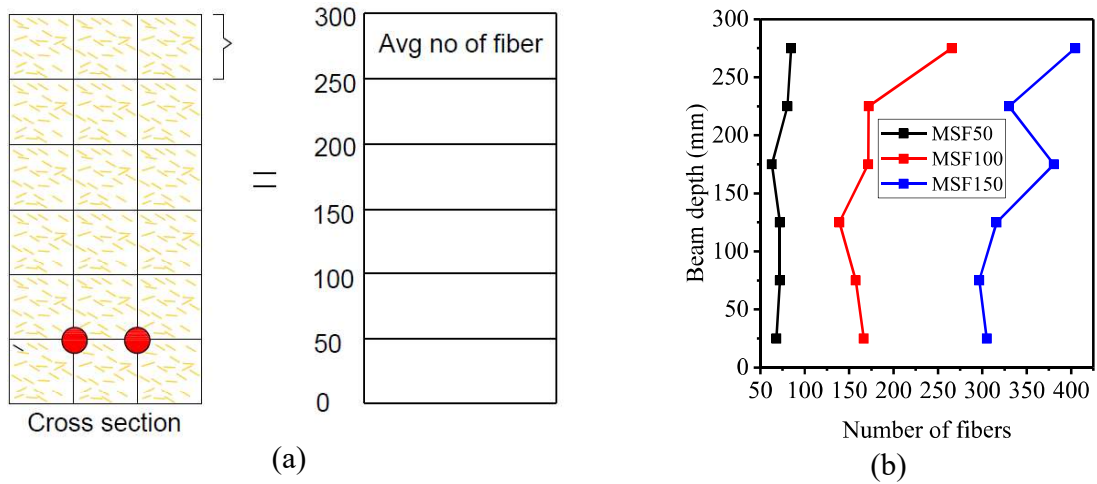


Figure 10. Fibre distribution across the depth of MSFRPC beam: (a) Grid with 50 mm x 50 mm spacing, (b) Average number of fibres across the depth

5.0 FINITE ELEMENT STUDIES

Three-dimensional FE models of test beams were created using finite element software ABAQUS. Concrete is modelled using C3D8R element with concrete damage plasticity model (CDP) as a material model. The prestressing strand and steel reinforcement were modelled using the truss element (T3D2). The stage-wise analysis is performed for prestressing and the applied shear loading.

5.1 Material Properties

Test specimens had an average compressive strength of 54 MPa, and the same is used for FE model. The stress-strain response of high-strength concrete without fibres in compression is modelled using the Thorenfeldt model[46]. Similarly, the stress-strain response of fibre reinforced concrete under compression is modelled using Yu-Chen et al. [47] model. The tension-stress strain behaviour is obtained from the inverse analysis developed by Bhosale et al. [42]. The stress-inelastic strain in both compression and tension for FRCs with different fibre dosages are shown in Figure 11.

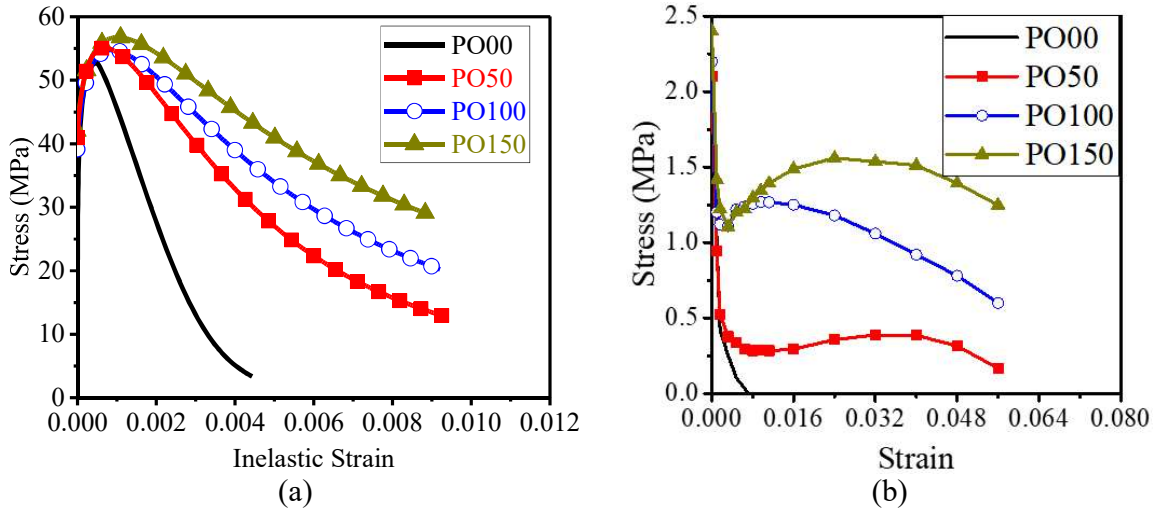


Figure 11. MSF concrete stress-strain properties: (a) Compression, (b) Tension

The damage in compression (d_c) and damage tension (d_t) is calculated as per **Equation (1)** - **Equation (2)** based on Huang and Liew [48]. The damage variables are a function of stress, elastic modulus, and strain in concrete.

$$d_c = 1 - \frac{\sigma_c + n_c f_{ck}}{E_c (n_c \sigma_c / E_c + \varepsilon_c)} \quad (1)$$

$$d_t = 1 - \frac{\sigma_t + n_t f_t}{E_c (n_t \sigma_t / E_c + \varepsilon_t)} \quad (2)$$

Where σ_c is stress, and f_{ck} is the compressive strength of concrete, E_c is the elastic modulus of concrete, n_c and n_t are the constant factors for compression and tension respectively, ε_c is the concrete strain in compression, and ε_t is concrete strain in tension which should be larger than zero.

The notched beams reinforced with macro synthetic fibre were tested. The fracture energy (G_f) is calculated as per JCI-S-001-2003[49]. The tensile strength from the inverse analysis [42] is used as tensile behaviour as input for concrete. The multi-linear stress-strain response obtained from inverse analysis (**Figure 11**) is used as input for inelastic strain and damage (d_t) parameters.

1
2
3
4
5
6
7
8
9
10
11
12
13
14
15
16
17
18
19
20
21
22
23
24
25
26
27
28
29
30
31
32
33
34
35
36
37
38
39
40
41
42
43
44
45
46
47
48
49
50
51
52
53
54
55
56
57
58
59
60
61
62
63
64
65

332 **5.2 Concrete Damage Plasticity Model (CDPM)**

333 The concrete damage plasticity model (CDPM) is widely used to represent the complex behaviour
334 of quasi-brittle material like concrete. This model is used for modelling concrete under both
335 monotonic and cyclic loading [27]. A three-dimensional eight-node element (C3D8R) in
336 ABAQUS is used for modelling concrete. The stress-strain response of concrete includes elastic
337 and plastic properties. The total strain of concrete is the combination of both elastic and plastic
338 strains. The nonlinear portion of the stress-strain response of concrete represents the plasticity and
339 damage response. Hence, it is essential to define the damage corresponding to the plastic strain of
340 concrete. The damage variables in concrete represented as d_c and d_t compression and tension
341 damage, respectively. The damage is identified in the range of 0 to 1. Here, 0 represents no-
342 damage, and 1 represents full damage [7,26,50–52]. The yield criteria define the critical stress
343 state beyond which plastic deformation initiates and leads to failure. Many researchers have
344 developed a yield criterion based on strength under compression and tension [27,28]. A similar
345 approach is adopted as CDPM in ABAQUS. Few researchers performed the test on concrete in
346 different conditions such as uniaxial tension, biaxial tension, uniaxial compression and biaxial
347 compression and developed failure envelopes [26,51]. For brevity, details on CDPM are not
348 provided here and can be found elsewhere (ABAQUS [53]).

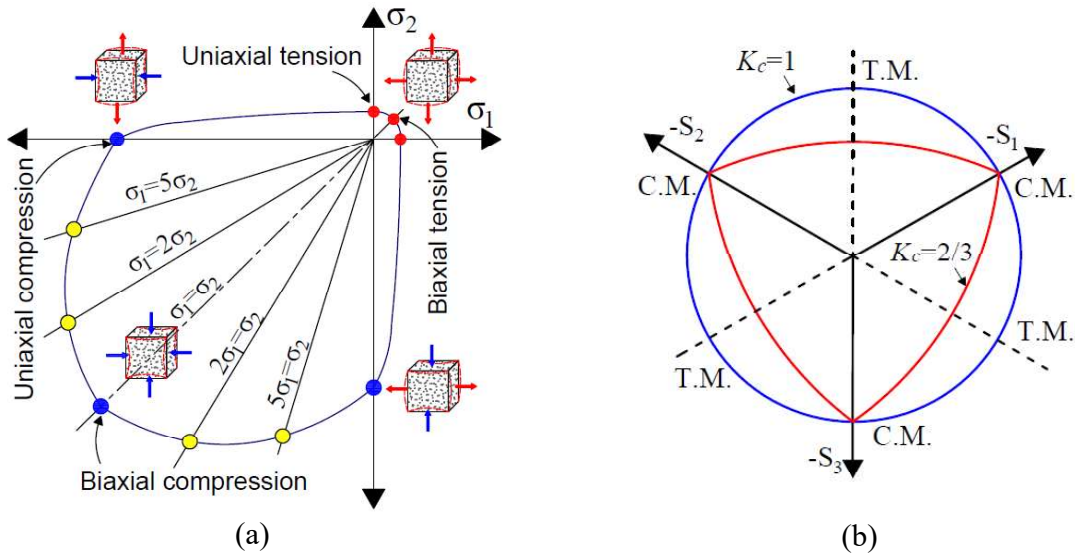


Figure 12. Yield criteria of concrete: (a) Concrete strength under biaxial stress, (b) Deviatoric cross-sections of the failure surface

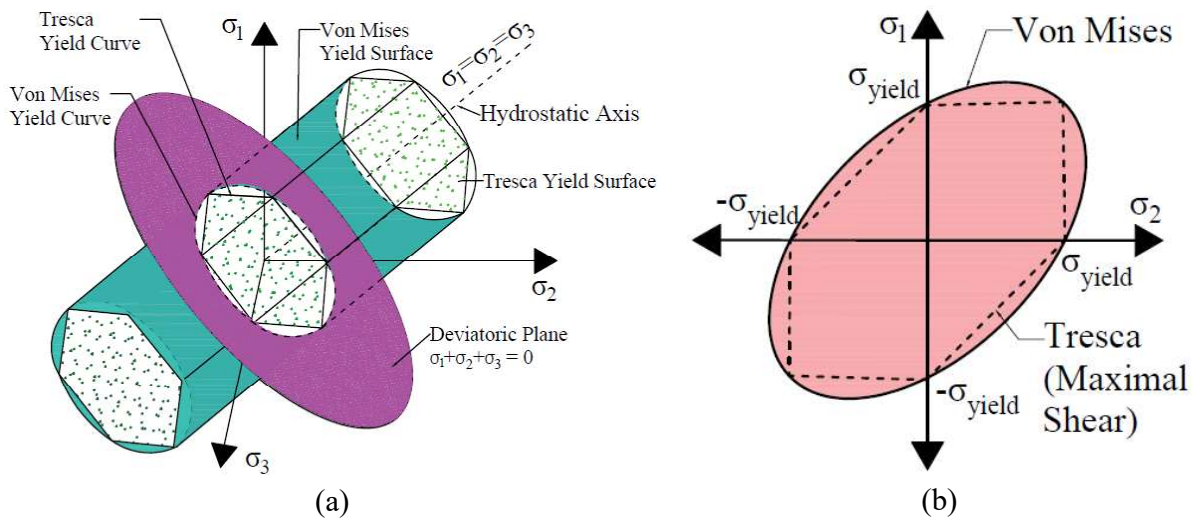


Figure 13. The different failure criterion for different stress models: (a) 3D schematic view, (b) Yield surface in 2D

The plasticity constants of concrete include dilation angle, eccentricity, stress ratio, shape factor, and viscosity parameter are shown in **Table 7**. The schematic view of yield criteria concrete and failure criteria are shown in **Figure 12** and **Figure 13**. Previous research shows that the dilation angle plays an important role in predicting peak load, post cracking behaviour, and failure mode

of beams [54–59]. From the sensitivity analysis, the dilation angle is chosen as 52.3° to simulate the experimental results closely. Other plasticity parameter values such as eccentricity, stress ratio, and shape factors are selected, such as default values. The analysis was carried out using ABAQUS/Standard, and the viscosity parameter term is activated [56]. The viscosity parameter is taken as 0.0005 for better convergence of the solution.

Table 7. Plasticity constants of concrete

Dilation angle (φ)	Eccentricity (ϵ)	F_{bo}/F_{co}	K_c	Viscosity Parameter (μ)
53.2°	0.1	1.16	0.667	0.0005

5.3 Prestressing Strands and Stirrups

The prestressing strand of length 1600 mm and with a cross-section of 98.4 mm^2 is modelled as a linear truss element (T3D2). The stress-strain properties of the strand were measured by a direct tension test, as shown in **Figure 6**, as explained in the experimental program. The same properties were converted as true stress-strain curve and implemented in FEM simulation. The pre-tensioning can be simulated by various modelling techniques such as initial stressing (default method). An initial prestress of 782.9 MPa is applied in each strand. The steel reinforcement of diameter 8 mm is used as secondary reinforcement. These secondary reinforcements were assigned with linear truss element (T3D2). The location of the stirrups and top reinforcement details are shown in **Figure 14 (a)**. Steel reinforcement is assumed to have elastic modulus ($E_{st} = 2 \times 10^5 \text{ MPa}$) and Poisson's ratio of 0.3. Both the high-strength prestressing strand and rebars were embedded in concrete. The embedment technique enables one or more elements to be embedded inside the host element. This technique does not require the modelling of the contact surface, and it eliminates the calculations of surface formulations [60]. The rebar node is defined as a master node, and

1
2
3
4
5
6
7
8
9
10
11
12
13
14
15
16
17
18
19
20
21
22
23
24
25
26
27
28
29
30
31
32
33
34
35
36
37
38
39
40
41
42
43
44
45
46
47
48
49
50
51
52
53
54
55
56
57
58
59
60
61
62
63
64
65

378 surrounding concrete is assigned as slave nodes, as shown in **Figure 14 (b)**. The rebar nodes lie in
379 the concrete element. Hence, the translation degrees of freedom of steel rebars is tied with that of
380 the concrete element.

381

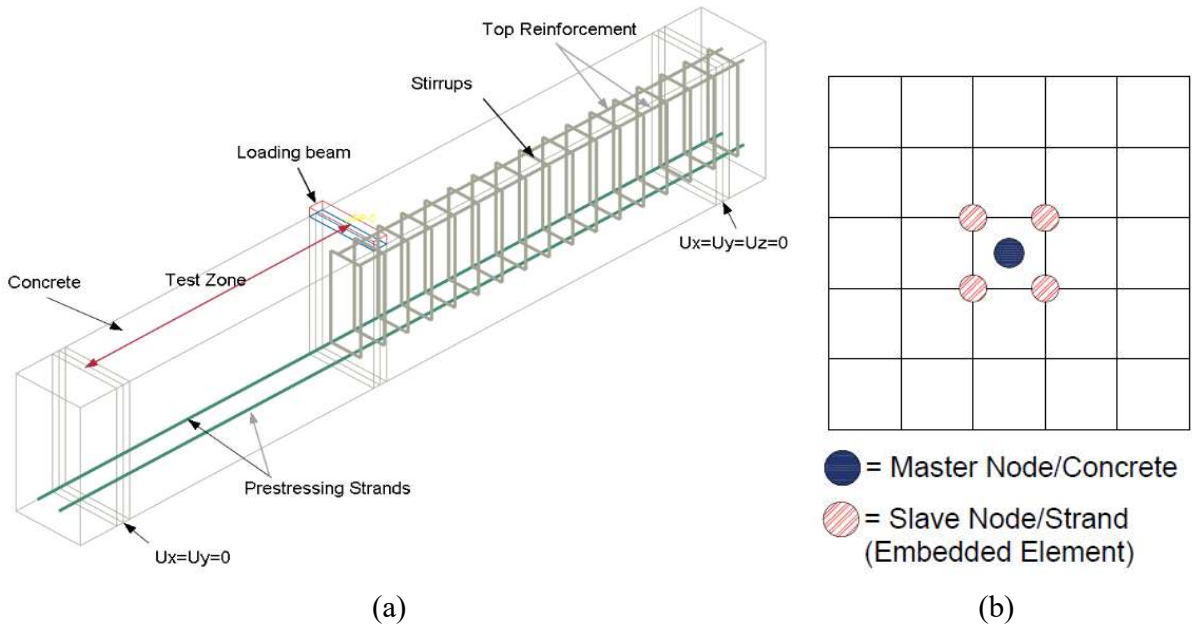


Figure 14. FE Modelling (a) Schematic view of prestressed concrete beam elements, (b) Strand slave nodes and concrete master nodes

382

5.4 Loading and Boundary Conditions

383

384 Loads were applied in two stages. The prestressing load was applied in the first stage, followed by
385 the external load in a displacement control mode. Simple support boundary conditions are imposed
386 in FEM modelling, as shown in **Figure 14 (a)**.

387

5.5 Load-Deflection Behaviour and Failure Modes

388

389 FE models of fibre-reinforced prestressed concrete beams with different dosages were developed
390 and analysed. The load-deflection behaviour and failure modes are shown in **Figure 15** and **Figure**
391 **16**, respectively. The load-deflection response of control (MSF00) and fibre reinforced concrete

1
2
3
4
5
6
7
8
9
10
11
12
13
14
15
16
17
18
19
20
21
22
23
24
25
26
27
28
29
30
31
32
33
34
35
36
37
38
39
40
41
42
43
44
45
46
47
48
49
50
51
52
53
54
55
56
57
58
59
60
61
62
63
64
65

392 beam (MSF50 and MSF100) is predicted well up to the ultimate load. In the case of MSF150 beam,
393 the load-deflection behaviour is little offset to that of observed behaviour. The failure mode of all
394 the prestressed concrete beams was in direct shear tension. The comparison between experimental
395 and FE simulation responses are shown in **Figure 16**.

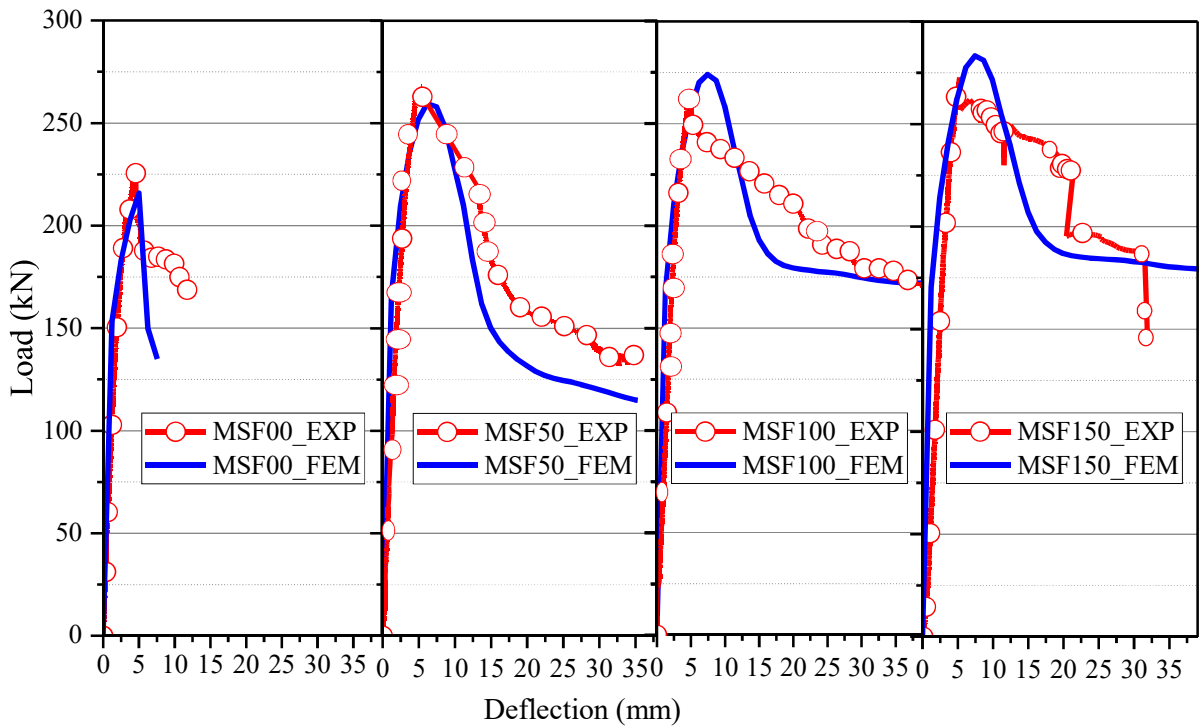


Figure 15. Load-deflection response of MSFRPC beams subjected to shear dominated loads

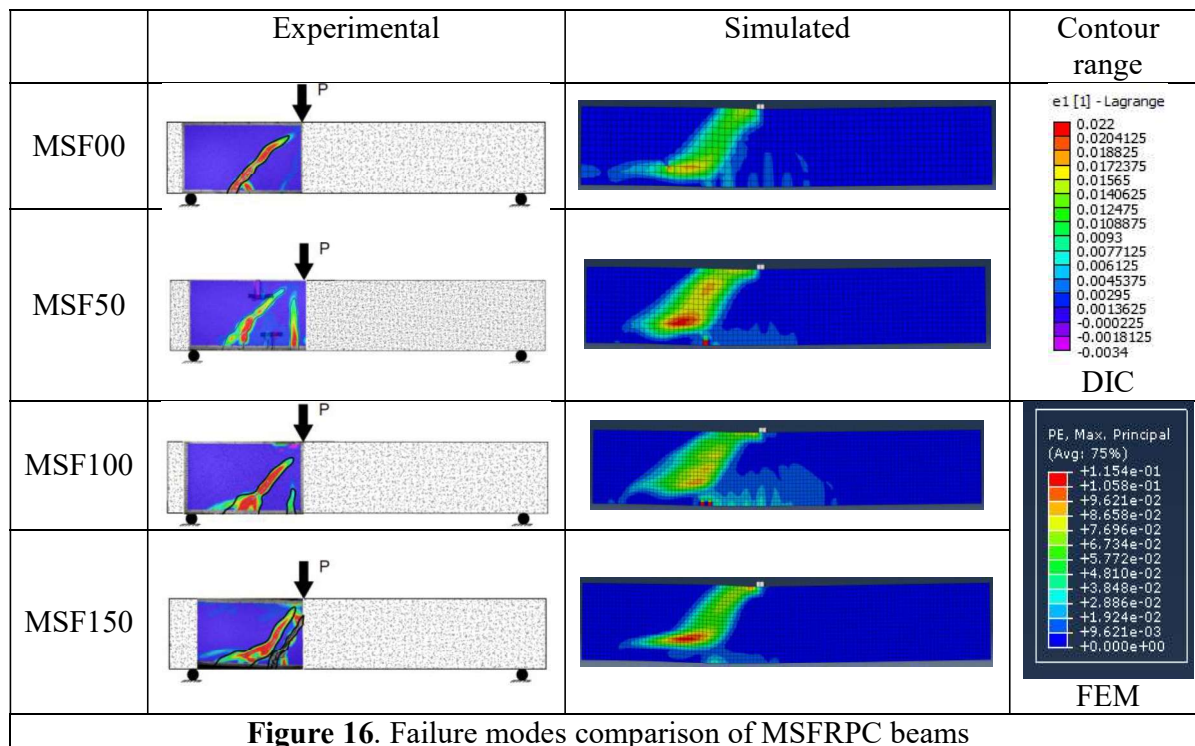


Figure 16. Failure modes comparison of MSFRPC beams

5.6 Parametric Studies

The shear capacity of prestressed fibre reinforced concrete beams depends on the concrete compressive strength, level of prestressing, shear reinforcement ratio, and fibre volume fraction.

Experimental validation of 0.0%, 0.5%, 1.0% and 1.5% volume fraction were studied. In this parametric study, the influence of the prestressing level is focused on the different volume fractions of fibres at the same shear span to depth ratio of 2.4. With the increase in the level of prestressing, the shear capacity of the beams increased, as shown in Figure 17.

The increase in the prestress level does not increase the shear strength significantly for the control beam (MSF00). For a higher prestress level of $0.8 P_u$, the specimen failed in a premature shear compression mode. In fibre-reinforced beams, a limited increase in shear strength (between 9% to 11%) was observed due to an increase in prestress levels. Figure 17 shows that there is not much

1
2
3
4
5
6
7
8
9
10
11
12
13
14
15
16
17
18
19
20
21
22
23
24
25
26
27
28
29
30
31
32
33
34
35
36
37
38
39
40
41
42
43
44
45
46
47
48
49
50
51
52
53
54
55
56
57
58
59
60
61
62
63
64
65

412 improvement in shear capacity after 60% of increment in prestressing. The MSFRPC beams of
 413 different levels of prestressing, such as 60%, 70%, and 80% failed in shear mode, as shown in
 414 **Figure 18**. The shear strength is enhancement is due to prestressing, which delayed the formation
 415 of shear cracks and helped in controlling the crack opening.

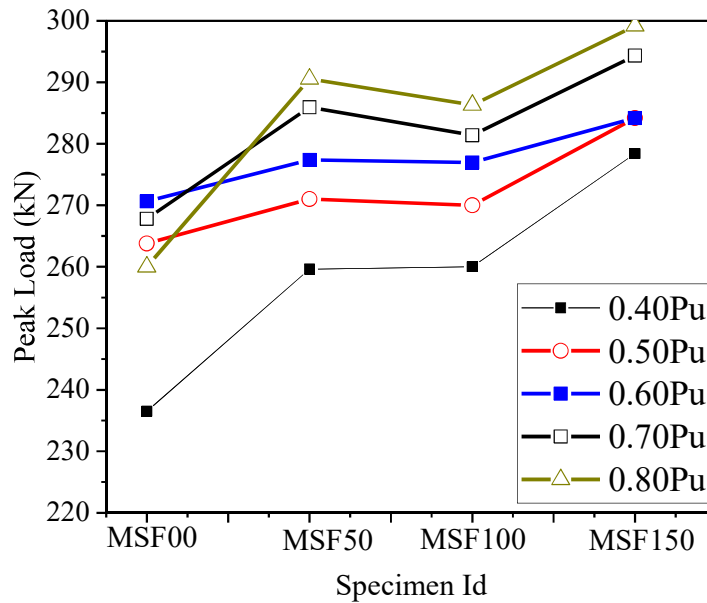


Figure 17. Parametric study on the level of prestressing

Beam ID	0.6P _u	0.7P _u	0.8P _u
MSF00			
MSF50			
MSF100			
MSF150			

Figure 18. Failure modes of MSFRPC beams at different level of prestressing

6.0 SHEAR CAPACITY PREDICTIONS BY RILEM AND FIB-MC2010 PROVISIONS

The shear capacity of MSFRPC beam is calculated by using RILEM [43] and Fib- MC2010 [61] code provisions. The average tensile strength of FRC as per RILEM provisions is used for estimating the shear capacity of beams.

6.1 Shear capacity calculations using RILEM recommendations (V_{RILEM})

The shear capacities (V_{RILEM}) formulations in RILEM recommendations [43] include three components such as shear resistance of member without shear reinforcement (V_{cd}), shear resistance due to discrete fibres (V_{fd}) and shear reinforcement/stirrup contribution (V_{wd}). The shear resistance of member without shear reinforcement (V_{cd}) includes the resistance due to un-cracked concrete, aggregate interlock, dowel action, and initial prestress. Similarly, shear resistance due to fibres (V_{fd}) includes factor accounting for the flange of T-sections and depth factor. The flange contribution is taken as one for rectangular beams. Other parameters were calculated as per the sectional details of the test specimens. The resistance offered by fibres in tension at a CMOD of 3.5 mm is used for shear contribution of fibres. These residual flexural tensile strengths vary based on fibre dosage and type of fibres and strength of concrete. The shear capacity of the tested MSFRPC beams using the RILEM equations are shown in **Figure 19**. Comparison of test results and predictions shows that the shear capacities of all the test specimens were conservatively estimated.

6.2 Shear Predictions using Fib-Model Code2010 Provisions (fib-MC2010)

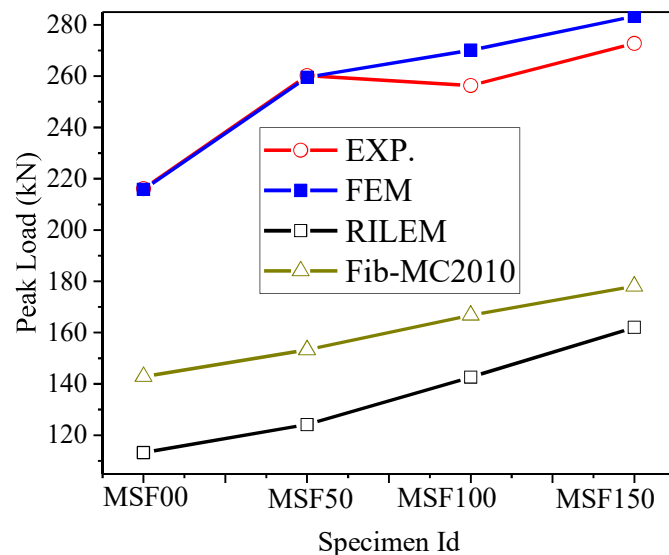
Fib-MC2010 code [61] explicitly includes several parameters in the shear capacity calculations ($V_{Rd,F}$). The parameters included in Fib-MC2010 for shear estimations include: (i) reinforcement

ratio of longitudinal bars (ρ_l), (ii) size effect factor which accounts the size influence on shear capacity of beam (K), (iii) concrete compressive strength (f_{ck}), (iv) average prestressing stress acting on the cross-section of concrete due to prestressing action (σ_{cp}), (v) fracture parameters such as ultimate residual tensile strength (f_{Ftuk}) and characteristic value of tensile strength of concrete matrix (f_{ctk}). The residual tensile strength of FRC was calculated at the CMODs of 0.5 mm and 2.5 mm. Based on the experimentally observed fracture test results (f_{R1} and f_{R3}), the residual tensile capacities (f_{Ftuk}) of different fibre dosages were calculated using the equations shown in **Table 8**. In these calculations, the partial safety factor of the concrete material is considered as 1. The obtained shear capacity of MSFRPC beams is shown in **Figure 19**.

Table 8. Shear capacity equations of RILEM recommendations and Fib-MC2010 provisions

Code	Capacity (V)	Theoretical Shear Capacity Formulas
RILEM	Concrete (V_{cd})	$V_{cd} = \left[0.12 k (100 \rho_l f_{ck})^{\frac{1}{3}} + 0.15 \sigma_{cp} \right] b d$, $k_l = k = 1 + \sqrt{\frac{200}{d}} \leq 2$ $k_f = 1 + n \left(\frac{h_f}{b_w} \right) \left(\frac{h_f}{d} \right) \leq 1.5$, $n = \left(\frac{b_f - b_w}{h_f} \right) \leq 3$, $\rho_l = \frac{A_s}{bd} \leq 0.002$
	Fibres (V_{fd})	$V_{fd} = 0.7 k_f k_l \tau_{fd} b d$, $\tau_{fd} = 0.12 f_{RK,4}$
	Prestress (σ_{cp})	$\sigma_{cp} = \left(\frac{N_{sd}}{A_c} \right)$
Fib-MC2010	Concrete ($V_{Rd,F}$)	$V_{Rd,F} = \left\{ 0.18 K \left[100 \rho_l \left(1 + 7.5 \frac{f_{Ftuk}}{f_{ctk}} \right) f_{ck} \right] + 0.15 \sigma_{cp} \right\}^{1/3} b_w d$ $f_{Ftu}(w_u) = f_{Fts} - \frac{w_u}{2.5} (f_{Fts} - 0.5 f_{R3} + 0.2 f_{R1}) \geq 0$ $f_{Fts} = 0.45 f_{R1}$, $f_{ck} = f_{cm} - 8$, $f_{ctm} = 0.3 f_{ck}^{2/3}$
	Prestress (σ_{cp})	$\sigma_{cp} = \left(\frac{N_{sd}}{A_c} \right)$

1
 2
 3
 4 454 The ratio of experimental to theoretically calculated shear capacity of MSFRPC beams is 1.5, 1.7,
 5
 6
 7 455 1.5, and 1.5 for MSF00, MSF50, MSF100, and MSF150, respectively. The prediction comparison
 8
 9 456 of fib-MC2010, RILEM, and FEM predictions show that the FEM results closely predict the test
 10
 11 457 results than the existing code provisions (**Figure 19**). Not many studies have focused on the
 12
 13
 14 458 performance improvement of prestressed concrete beams under shear through macro synthetic
 15
 16 459 fibre addition. More experimental research on macro-synthetic fibre reinforced concrete beams
 17
 18
 19 460 under shear loads for a wide range of parameters is required to develop a rational shear capacity
 20
 21 461 model for design purposes. It is a scope for future work.
 22
 23
 24 462



25
 26
 27
 28
 29
 30
 31
 32
 33
 34
 35
 36
 37
 38
 39
 40
 41
 42
 43
 44
 45 **Figure 19.** Comparison of shear capacity predictions with experimental and FEM predictions
 46

47 463
 48
 49 464 **7.0 SUMMARY AND CONCLUSIONS**
 50

51 465 The shear behaviour of MSFRPC concrete beams was studied through experimental and numerical
 52
 53
 54 466 means. The effect of volume fraction of macro synthetic fibres was considered. Tension stress-
 55
 56 467 strain response of macro synthetic FRC obtained from the inverse analysis was used as input for
 57
 58
 59 468 FEM analysis. The nonlinear three-dimensional finite element models were developed, and the
 60
 61
 62
 63
 64
 65

1
2
3
4 469 predictions were validated with test results. The load-deflection response and failure modes were
5
6
7 470 compared with FEM results. After that, a detailed parametric study was performed by varying the
8
9 471 level of prestressing. Based on this limited study, the following conclusions can be drawn:

- 11 472 1. The fracture test results revealed that the macro synthetic fibres are effective at higher crack
12
13
14 473 opening displacements higher than 2.5mm. Due to addition of macro synthetic fibers of 1.0%
15
16 474 and 1.5% of volume fractions, the fracture energy increased by 9.6 and 16 times compared to
17
18
19 475 control specimen.
- 21 476 2. The failure mode of prestressed concrete beams changed from brittle to ductile mode due to
22
23
24 477 the addition of fibres at 0.5%, 1%, and 1.5%. The energy absorption capacity increased by
25
26 478 3.7, 4 and 6 times for 0.5%, 1.0% and 1.5% volume of fibre addition.
- 28 479 3. The predictions of load-deflection and failure mode using the finite element approach adopted
29
30
31 480 in this study closely matched the test results. Parametric studies showed that the shear capacity
32
33
34 481 of prestressed concrete beams increased by up to 18 % with an increase in fibre dosage and
35
36 482 up to 15% due to increase in level of prestressing.
- 38 483 4. The shear capacity estimations by RILEM and fib-MC2010 code predictions are very
39
40
41 484 conservative compared to FE predictions. More research is required on macro-synthetic fiber
42
43 485 reinforced concrete beams to improve the existing code provisions.
44
45
46 486

48 487 **8.0 ACKNOWLEDGEMENTS**

50 488 The authors would like to acknowledge the financial support from the Ministry of Tribal Affairs
51
52
53 489 India through Award No: 201920-NFST-TEL-01354, Utchattar Avishkar Yojana (UAY) Scheme,
54
55 490 Government of India through Grant No: UAY-IITH_008, and PRECA India Pvt. Ltd. for
56
57
58
59
60
61
62
63
64
65

1
2
3
4
5
6
7
8
9
10
11
12
13
14
15
16
17
18
19
20
21
22
23
24
25
26
27
28
29
30
31
32
33
34
35
36
37
38
39
40
41
42
43
44
45
46
47
48
49
50
51
52
53
54
55
56
57
58
59
60
61
62
63
64
65

491 sponsoring the materials required for this research. Specimens were cast at the precast yard of
492 PRECA India Pvt. Ltd.

493

494 **9.0 CONFLICTS OF INTEREST**

495 None.

496

497 **10.0 DATA AVAILABILITY STATEMENT**

498 Some or all data and models that support the findings of this study are available from the
499 corresponding author upon reasonable request.

500

501 **11.0 REFERENCES**

502 [1] B.A. Graybeal, Flexural behavior of an ultrahigh-performance concrete I-girder, *J. Bridg.*
503 *Eng.* 13 (2008) 602–610. [https://doi.org/10.1061/\(ASCE\)1084-0702\(2008\)13:6\(602\)](https://doi.org/10.1061/(ASCE)1084-0702(2008)13:6(602)).
504 [2] D.B. Garber, J.M. Gallardo, D.J. Deschenes, O. Bayrak, Nontraditional Shear Failures in
505 Bulb-T Prestressed Concrete Bridge Girders, *J. Bridg. Eng.* 21 (2016) 1–10.
506 [https://doi.org/10.1061/\(ASCE\)BE.1943-5592.0000890](https://doi.org/10.1061/(ASCE)BE.1943-5592.0000890).
507 [3] G.P. Osborn, P.J. Barr, D.A. Petty, M.W. Halling, T.R. Brackus, Residual prestress forces
508 and shear capacity of salvaged prestressed concrete bridge girders, *J. Bridg. Eng.* 17 (2012)
509 302–309. [https://doi.org/10.1061/\(ASCE\)BE.1943-5592.0000212](https://doi.org/10.1061/(ASCE)BE.1943-5592.0000212).
510 [4] K.H. Tan, F.K. Kong, L.W. Weng, High-strength reinforced concrete deep and short beams:
511 Shear design equations in North American and UK practice, *ACI Struct. J.* 95 (1998) 318–
512 329. <https://doi.org/10.14359/549>.
513 [5] W. Ji, W. Li, M. An, L. Zhu, Shear Capacity of T-Section Girders Made of Reactive Powder

- 1
2
3
4 514 Concrete, *J. Bridg. Eng.* 23 (2018) 1–20. [https://doi.org/10.1061/\(ASCE\)BE.1943-](https://doi.org/10.1061/(ASCE)BE.1943-)
5
6 515 5592.0001253.
7
8
9 516 [6] S.J. Hwang, W.Y. Lu, H.J. Lee, Shear strength prediction for deep beams, *ACI Struct. J.* 97
10
11 517 (2000) 367–376. <https://doi.org/10.14359/9624>.
12
13
14 518 [7] Y. Chi, M. Yu, L. Huang, L. Xu, Finite element modeling of steel-polypropylene hybrid
15
16 519 fiber reinforced concrete using modified concrete damaged plasticity, *Eng. Struct.* 148
17
18 520 (2017) 23–35. <https://doi.org/10.1016/j.engstruct.2017.06.039>.
19
20
21 521 [8] S. Gali, K.V.L. Subramaniam, Shear behavior of slender and non-slender steel fiber-
22
23 522 reinforced concrete beams, *ACI Struct. J.* 116 (2019) 149–158.
24
25 523 <https://doi.org/10.14359/51713307>.
26
27
28 524 [9] S.J. Foster, A. Agarwal, A. Amin, Design of steel fiber reinforced concrete beams for shear
29
30 525 using inverse analysis for determination of residual tensile strength, *Struct. Concr.* 19 (2018)
31
32 526 129–140. <https://doi.org/10.1002/suco.201700100>.
33
34
35 527 [10] D.R. Sahoo, A. Solanki, A. Kumar, Influence of steel and polypropylene fibers on flexural
36
37 528 behavior of RC beams, *J. Mater. Civ. Eng.* 27 (2015) 1–9.
38
39 529 [https://doi.org/10.1061/\(ASCE\)MT.1943-5533.0001193](https://doi.org/10.1061/(ASCE)MT.1943-5533.0001193).
40
41
42 530 [11] W. Kaufmann, A. Amin, A. Beck, M. Lee, Shear transfer across cracks in steel fibre
43
44 531 reinforced concrete, *Eng. Struct.* 186 (2019) 508–524.
45
46 532 <https://doi.org/10.1016/j.engstruct.2019.02.027>.
47
48
49 533 [12] A. Amin, S.J. Foster, Shear strength of steel fibre reinforced concrete beams with stirrups,
50
51 534 *Eng. Struct.* 111 (2016) 323–332. <https://doi.org/10.1016/j.engstruct.2015.12.026>.
52
53
54 535 [13] A. Dev, M. Chellapandian, S.S. Prakash, Effect of Macrosynthetic and Hybrid Fibers on
55
56 536 Shear Behavior of Concrete Beams Reinforced with GFRP Bars, *J. Bridg. Eng.* 25 (2020)
57
58
59
60
61
62
63
64
65

1
2
3
4
5
6
7
8
9
10
11
12
13
14
15
16
17
18
19
20
21
22
23
24
25
26
27
28
29
30
31
32
33
34
35
36
37
38
39
40
41
42
43
44
45
46
47
48
49
50
51
52
53
54
55
56
57
58
59
60
61
62
63
64
65

537 1–16. [https://doi.org/10.1061/\(ASCE\)BE.1943-5592.0001557](https://doi.org/10.1061/(ASCE)BE.1943-5592.0001557).

538 [14] J.A. McMahon, A.C. Birely, Experimental Performance of Steel Fiber Reinforced Concrete
539 Bridge Deck, *J. Bridg. Eng.* 23 (2018) 1–14. [https://doi.org/10.1061/\(ASCE\)BE.1943-5592.0001287](https://doi.org/10.1061/(ASCE)BE.1943-5592.0001287).

540

541 [15] E. Cuenca, P. Serna, Shear behavior of prestressed precast beams made of self-compacting
542 fiber reinforced concrete, *Constr. Build. Mater.* 45 (2013) 145–156.
543 <https://doi.org/10.1016/j.conbuildmat.2013.03.096>.

544 [16] ACI Committee 318, Building Code Requirements Available for Public Review (ACI 318-
545 19), 2019.

546 [17] J.S. Cho, J. Lundy, S.H. Chao, Shear strength of steel fiber reinforced prestressed concrete
547 beams, *Proc. 2009 Struct. Congr. - Don't Mess with Struct. Eng. Expand. Our Role.* (2009)
548 1058–1066. [https://doi.org/10.1061/41031\(341\)117](https://doi.org/10.1061/41031(341)117).

549 [18] C. Lakavath, S.S. Joshi, S.S. Prakash, Investigation of the effect of steel fibers on the shear
550 crack-opening and crack-slip behavior of prestressed concrete beams using digital image
551 correlation, *Eng. Struct.* 193 (2019) 28–42.
552 <https://doi.org/10.1016/J.ENGSTRUCT.2019.05.030>.

553 [19] M.A. Rasheed, S.S. Prakash, Behavior of hybrid-synthetic fiber reinforced cellular
554 lightweight concrete under uniaxial tension – Experimental and analytical studies, *Constr.*
555 *Build. Mater.* 162 (2018) 857–870. <https://doi.org/10.1016/j.conbuildmat.2017.12.095>.

556 [20] M.A. Rasheed, S.S. Prakash, Mechanical behavior of sustainable hybrid-synthetic fiber
557 reinforced cellular light weight concrete for structural applications of masonry, *Constr.*
558 *Build. Mater.* 98 (2015) 631–640. <https://doi.org/10.1016/j.conbuildmat.2015.08.137>.

559 [21] A. Bhosale, M.A. Rasheed, S.S. Prakash, G. Raju, A study on the efficiency of steel vs.

1
2
3
4
5
6
7
8
9
10
11
12
13
14
15
16
17
18
19
20
21
22
23
24
25
26
27
28
29
30
31
32
33
34
35
36
37
38
39
40
41
42
43
44
45
46
47
48
49
50
51
52
53
54
55
56
57
58
59
60
61
62
63
64
65

560 synthetic vs. hybrid fibers on fracture behavior of concrete in flexure using acoustic
561 emission, *Constr. Build. Mater.* 199 (2019) 256–268.
562 <https://doi.org/10.1016/j.conbuildmat.2018.12.011>.

[22] A. Conforti, F. Minelli, A. Tinini, G.A. Plizzari, Influence of polypropylene fibre
563 reinforcement and width-to-effective depth ratio in wide-shallow beams, *Eng. Struct.* 88
564 (2015) 12–21. <https://doi.org/10.1016/j.engstruct.2015.01.037>.

[23] M.N. Soutsos, T.T. Le, A.P. Lampropoulos, Flexural performance of fibre reinforced
565 concrete made with steel and synthetic fibres, *Constr. Build. Mater.* 36 (2012) 704–710.
566 <https://doi.org/10.1016/j.conbuildmat.2012.06.042>.

[24] B. Boulekbache, M. Hamrat, M. Chemrouk, S. Amziane, Influence of yield stress and
567 compressive strength on direct shear behaviour of steel fibre-reinforced concrete, *Constr.*
568 *Build. Mater.* 27 (2012) 6–14. <https://doi.org/10.1016/j.conbuildmat.2011.07.015>.

[25] N. Buratti, C. Mazzotti, M. Savoia, Post-cracking behaviour of steel and macro-synthetic
569 fibre-reinforced concretes, *Constr. Build. Mater.* 25 (2011) 2713–2722.
570 <https://doi.org/10.1016/j.conbuildmat.2010.12.022>.

[26] Y. Chi, L. Xu, H. sui Yu, Constitutive modeling of steel-polypropylene hybrid fiber
571 reinforced concrete using a non-associated plasticity and its numerical implementation,
572 *Compos. Struct.* 111 (2014) 497–509. <https://doi.org/10.1016/j.compstruct.2014.01.025>.

[27] J. Lee, G.L. Fenves, ASCE, Plastic-Damage Model for Cyclic Loading of Concrete
573 Structures, *J. Eng. Mech.* 124 (1998) 892–900.

[28] J. Lubliner, J. Oliver, S. Oller, E. Onate, a Plastic-Damage Model, *Int. J. Solids Struct.* 25
574 (1989) 299–326.

[29] S.J. Stephen, B. Raphael, R. Gettu, S. Jose, Determination of the tensile constitutive

1
2
3
4
5
6
7
8
9
10
11
12
13
14
15
16
17
18
19
20
21
22
23
24
25
26
27
28
29
30
31
32
33
34
35
36
37
38
39
40
41
42
43
44
45
46
47
48
49
50
51
52
53
54
55
56
57
58
59
60
61
62
63
64
65

583 relations of fiber reinforced concrete using inverse analysis, *Constr. Build. Mater.* 195
584 (2019) 405–414. <https://doi.org/10.1016/j.conbuildmat.2018.11.014>.

585 [30] G. Kani, How Safe are Our Large Reinforced Concrete Beams?, *ACI J. Proc.* 64 (1967).
586 <https://doi.org/10.14359/7549>.

587 [31] M. Shahnewaz, M.S. Alam, Improved shear equations for steel fiber-reinforced concrete
588 deep and slender beams, *ACI Struct. J.* 111 (2014) 851–860.
589 <https://doi.org/10.14359/51686736>.

590 [32] B.I. Mihaylov, J. Liu, K. Simionopoulos, E.C. Bentz, M.P. Collins, Effect of member size
591 and tendon layout on shear behavior of post-tensioned beams, *ACI Struct. J.* 116 (2019)
592 265–274. <https://doi.org/10.14359/51715633>.

593 [33] Bureau of Indian Standards, IS 10262- 2019, Concrete mix proportioning- guidelines,
594 (2019) 1–40.

595 [34] A. Enfedaque, M.G. Alberti, J.C. Gálvez, Influence of fiber distribution and orientation in
596 the fracture behavior of polyolefin fiber-reinforced concrete, *Materials (Basel)*. 12 (2019).
597 <https://doi.org/10.3390/ma12020220>.

598 [35] S.T. Kang, J.K. Kim, The relation between fiber orientation and tensile behavior in an ultra
599 high performance fiber reinforced cementitious composites (UHPFRCC), *Cem. Concr. Res.*
600 41 (2011) 1001–1014. <https://doi.org/10.1016/j.cemconres.2011.05.009>.

601 [36] F. Laranjeira, A. Aguado, C. Molins, S. Grünewald, J. Walraven, S. Cavalaro, Framework
602 to predict the orientation of fibers in FRC: A novel philosophy, *Cem. Concr. Res.* 42 (2012)
603 752–768. <https://doi.org/10.1016/j.cemconres.2012.02.013>.

604 [37] A. Abrishambaf, M. Pimentel, S. Nunes, Influence of fibre orientation on the tensile
605 behaviour of ultra-high performance fibre reinforced cementitious composites, *Cem. Concr.*

1
2
3
4
5
6
7
8
9
10
11
12
13
14
15
16
17
18
19
20
21
22
23
24
25
26
27
28
29
30
31
32
33
34
35
36
37
38
39
40
41
42
43
44
45
46
47
48
49
50
51
52
53
54
55
56
57
58
59
60
61
62
63
64
65

606 Res. 97 (2017) 28–40. <https://doi.org/10.1016/j.cemconres.2017.03.007>.

607 [38] F.Y. Li, L.Y. Li, Y. Dang, P.F. Wu, Study of the effect of fibre orientation on artificially
608 directed steel fibre-reinforced concrete, *Adv. Mater. Sci. Eng.* 2018 (2018).
609 <https://doi.org/10.1155/2018/8657083>.

610 [39] F. Laranjeira, S. Grünwald, J. Walraven, C. Blom, C. Molins, A. Aguado, Characterization
611 of the orientation profile of steel fiber reinforced concrete, *Mater. Struct. Constr.* 44 (2011)
612 1093–1111. <https://doi.org/10.1617/s11527-010-9686-5>.

613 [40] I. Şanal, N. Özyurt Zihnioğlu, To what extent does the fiber orientation affect mechanical
614 performance?, *Constr. Build. Mater.* 44 (2013) 671–681.
615 <https://doi.org/10.1016/j.conbuildmat.2013.03.079>.

616 [41] G. Srikar, G. Anand, S.S. Prakash, A Study on Residual Compression Behavior of Structural
617 Fiber Reinforced Concrete Exposed to Moderate Temperature Using Digital Image
618 Correlation, *Int. J. Concr. Struct. Mater.* 10 (2016) 75–85. <https://doi.org/10.1007/s40069-016-0127-x>.

619
620 [42] A.B. Bhosale, C. Lakavath, S. Suriya Prakash, Multi-linear tensile stress-crack width
621 relationships for hybrid fibre reinforced concrete using inverse analysis and digital image
622 correlation, *Eng. Struct.* 225 (2020) 111275.
623 <https://doi.org/10.1016/j.engstruct.2020.111275>.

624 [43] L. Vandewalle, D. Nemegeer, G.L. Balazs, B. Barr, P. Bartos, N. Banthia, A.M. Brandt, M.
625 Criswell, F. Denarie, M. di Prisco, H. Falkner, R. Gettu, V. Gopalaratnam, P. Groth, V.
626 Hausler, F. Katsaragafis, A. Kooiman, K. Kovler, J. Lehtonen, B. Massicotte, S. Mindess,
627 H. Reinhardt, P. Rossi, S. Schaerlaekens, B. Schnutgen, S. Shah, A. Skarendahl, H. Stang,
628 P. Stroeven, R. Swamy, P. Tatnall, M. Teutsch, J. Walraven, A. Wubs, *Rilem TC 162-TDF*:

1
2
3
4
5
6
7
8
9
10
11
12
13
14
15
16
17
18
19
20
21
22
23
24
25
26
27
28
29
30
31
32
33
34
35
36
37
38
39
40
41
42
43
44
45
46
47
48
49
50
51
52
53
54
55
56
57
58
59
60
61
62
63
64
65

629 Test and design methods for steel fibre reinforced concrete: Uni-axial tension test for steel
630 fibre reinforced concrete, *Mater. Struct. Constr.* 34 (2001) 3–6.
631 <https://doi.org/10.1617/13628>.

[44] JCI-S-002-2003, Method of test for load-displacement curve of fiber reinforced concrete by
632 use of notched beam, (2003) 3–8.

[45] ASTM International., 1061/A1061M-09 Standard Test Methods for Testing Multi-Wire
633 Steel Strand., West Conshohocken, PA; ASTM Int. (2009).
634 https://doi.org/https://doi.org/10.1520/A1061_A1061M-09.

[46] A. Thorenfeldt, E. Tomaszewicz, J.J. Jensen, Mechanical Properties of High-
635 strengthConcrete and Application in Design, in: *Proc. Symp. Util. High-StrengthConcrete*,
636 Tapir, Trondheim, 1987: pp. 149–159.

[47] Y.C. Ou, M. Sen Tsai, K.Y. Liu, K.C. Chang, Compressive Behavior of Steel-Fiber-
637 Reinforced Concrete with a High Reinforcing Index, *J. Mater. Civ. Eng.* 24 (2012) 207–
638 215. [https://doi.org/10.1061/\(ASCE\)MT.1943-5533.0000372](https://doi.org/10.1061/(ASCE)MT.1943-5533.0000372).

[48] Z. Huang, J.Y.R. Liew, Nonlinear finite element modelling and parametric study of curved
639 steel-concrete-steel double skin composite panels infilled with ultra-lightweight cement
640 composite, *Constr. Build. Mater.* 95 (2015) 922–938.
641 <https://doi.org/10.1016/j.conbuildmat.2015.07.134>.

[49] JCI-S-001-2003, Method of test for fracture energy of concrete by use of notched beam, 2
642 (2003) 1–14.

[50] T. Yu, J.G. Teng, Y.L. Wong, S.L. Dong, Finite element modeling of confined concrete-II:
643 Plastic-damage model, *Eng. Struct.* 32 (2010) 680–691.
644 <https://doi.org/10.1016/j.engstruct.2009.11.013>.

1
2
3
4
5
6
7
8
9
10
11
12
13
14
15
16
17
18
19
20
21
22
23
24
25
26
27
28
29
30
31
32
33
34
35
36
37
38
39
40
41
42
43
44
45
46
47
48
49
50
51
52
53
54
55
56
57
58
59
60
61
62
63
64
65

[51] Y. Chi, L. Xu, H.S. Yu, Plasticity model for hybrid fiber-reinforced concrete under true triaxial compression, *J. Eng. Mech.* 140 (2014) 393–405. [https://doi.org/10.1061/\(ASCE\)EM.1943-7889.0000659](https://doi.org/10.1061/(ASCE)EM.1943-7889.0000659).

[52] C. Lakavath, M.S.V. Sagi, S.S. Joshi, S.S. Prakash, Finite element studies on the flexure-shear behavior of steel and hybrid fiber reinforced prestressed concrete beams, *Indian Concr. J.* 95 (2021) 58–70.

[53] Abaqus 6.11, Abaqus 6.11. Dassault Systemes Simulia Corp Providence, (2011).

[54] T. Rahman, W. Lutz, R. Finn, S. Schmauder, S. Aicher, Simulation of the mechanical behavior and damage in components made of strain softening cellulose fiber reinforced gypsum materials, *Comput. Mater. Sci.* 39 (2007) 65–74. <https://doi.org/10.1016/j.commatsci.2006.01.032>.

[55] A.S. Genikomsou, M.A. Polak, Finite element analysis of punching shear of concrete slabs using damaged plasticity model in ABAQUS, *Eng. Struct.* 98 (2015) 38–48. <https://doi.org/10.1016/j.engstruct.2015.04.016>.

[56] A. Wosatko, A. Winnicki, M.A. Polak, J. Pamin, Role of dilatancy angle in plasticity-based models of concrete, *Arch. Civ. Mech. Eng.* 19 (2019) 1268–1283. <https://doi.org/10.1016/j.acme.2019.07.003>.

[57] M. Lapi, L. Secci, E. Teoni, A.P. Ramos, M. Orlando, A hybrid method for the calibration of finite element models of punching-shear in R/C flat slabs, *Comput. Struct.* 238 (2020) 106323. <https://doi.org/10.1016/j.compstruc.2020.106323>.

[58] A. Earij, G. Alfano, K. Cashell, X. Zhou, Nonlinear three-dimensional finite-element modelling of reinforced-concrete beams: Computational challenges and experimental validation, *Eng. Fail. Anal.* 82 (2017) 92–115.

1
2
3
4
5
6
7
8
9
10
11
12
13
14
15
16
17
18
19
20
21
22
23
24
25
26
27
28
29
30
31
32
33
34
35
36
37
38
39
40
41
42
43
44
45
46
47
48
49
50
51
52
53
54
55
56
57
58
59
60
61
62
63
64
65

675 <https://doi.org/10.1016/j.engfailanal.2017.08.025>.

676 [59] J.G. Stoner, Finite Element Modelling of GFRP Reinforced, University of Waterloo, 2015.

677 [60] A.A. Arab, S.S. Badie, M. T., A methodological approach for finite element modeling of
678 pretensioned concrete members at the release of pretensioning, Eng. Struct. 33 (2011) 1918–
679 1929. <https://doi.org/10.1016/j.engstruct.2011.02.028>.

680 [61] Model Code 2010-First complete draft-Volume 2: Model Code. Vol. 56., Fédération
681 Internationale du Béton (fib), 2010.

682